Stellar Capture Rates in Galactic Nuclei Containing a Supermassive Binary Black Hole

A THESIS
SUBMITTED FOR THE DEGREE OF
Bachelor of Science (Research)

BY

Shashank Dattathri
Undergraduate Department
Indian Institute of Science

UNDER THE SUPERVISION OF

Prof. Arun Mangalam
Indian Institute of Astrophysics

AND

Prof. Nirupam Roy
Department of Physics
Indian Institute of Science

Indian Institute of Science
Bangalore – 560 012 (INDIA)

June, 2020

Declaration of Originality

I, **Shashank Dattathri**, with SR No. **11-01-00-10-91-16-1-13799** hereby declare that the material presented in the thesis titled

Stellar Capture Rates in Galactic Nuclei Containing a Supermassive Binary Black Hole

represents original work carried out by me from **June 2019** to **June 2020**.
With my signature, I certify that:

- I have not manipulated any of the data or results.
- I have not committed any plagiarism of intellectual property. I have clearly indicated and referenced the contributions of others.
- I have explicitly acknowledged all collaborative research and discussions.
- I have understood that any false claim will result in severe disciplinary action.
- I have understood that the work may be screened for any form of academic misconduct.

Date: 28/06/2020

Student Signature

In my capacity as supervisor of the above-mentioned work, I certify that the above statements are true to the best of my knowledge, and I have carried out due diligence to ensure the originality of the report.

Advisor Signature
Arun Mangalam
Professor
Indian Institute of Astrophysics

Acknowledgments

Working on this project gave me many new insights into the world of research, and I owe an immense debt of gratitude to a number of people and institutions.
First and foremost, I thank Prof. Arun Mangalam for being my thesis advisor, and for his constant support during my project. Working with him was an incredible experience, and every discussion we had was fruitful and intellectually stimulating. In addition, I thank Prof. Nirupam Roy for being my home institution adviser. He was very approachable and willing to give me time when I needed it.
Of course, I thank the UG program at IISc for giving me the time and opportunity to work on such a long-term project during my undergraduate days. In addition, I thank the Visiting Students Internship Program at IIA for providing me the opportunity to work at IIA.
Finally, I thank my friends and family for their constant support and encouragement.

Abstract

We study the stellar capture rates in galactic nuclei containing a supermassive black hole binary with unequal masses. A hierarchical system of a primary supermassive black hole (SMBH), a secondary SMBH, and a field star in a power-law cusp around the primary is considered. The stellar dynamics of the field stars is influenced by secondary black hole, the stellar cusp, and general relativity. The secondary SMBH inspirals towards the primary under the effects of dynamical friction and slingshot mechanisms. There is a small period of time during the binary evolution when a field star exhibits angular momentum oscillations similar to the Lidov-Kozai mechanism in celestial mechanics. These oscillations can greatly increase the feeding into the loss cone. We develop a model for the stellar dynamics of the field stars and the capture rate over time.

Our results show that the capture rate enters an enhanced phase when the binary separation is $\sim 0.1 - 1$ pc. The peak rate during this time is of the order 10^{-2} $M_\odot$ yr^{-1}, which is two to three orders of magnitude higher compared to isolated SMBH rates. This enhanced phase lasts for a period of $\sim 10^5 - 10^6$ yr. The dependence of the peak rate and duration of enhancement on the mass of the primary SMBH, the mass ratio, and the stellar cusp profile is discussed. The enhanced rate of tidal disruption events can serve as a powerful observational tool in identifying minor mergers.

Contents

List of Figures

List of Tables

Glossary

Table 1: List of symbols used

M_1	Mass of primary black hole
M_2	Mass of secondary black hole
q	Mass ratio (also used unambiguously in sections 2.2.2 and 2.2.3 to denote a dimensionless variable)
γ	Density power law index
p	$= \gamma - 3/2$
σ	Stellar velocity dispersion
m_*	Mass of field star
r_h	Radius of influence of M_1
r_0	Radius of cusp
η	$= r_h/r_0$
a_h	Binary hardening radius
ρ_0	Density of stars at r_0
H	Hamiltonian
$\mathcal{H}$	Binary hardening rate
ω	Argument of pericenter
e	Eccentricity
T_K	Kozai timescale
D_{max}	Starting binary separation of enhanced phase
D_{min}	Ending binary separation of enhanced phase
N_p	Peak capture rate
D_p	Binary separation at peak capture rate
T_e	Duration of enhanced phase

Chapter 1

Introduction

Supermassive black holes exist at the nucleus of nearly all galaxies. The study of the properties of SMBHs, their effects on the surrounding star cluster, and most importantly, their detection has been an active and rapidly evolving topic of research. Systems containing SMBHs exhibit many extraordinary phenomena: the inspiral of massive objects lead to emission of gravitational waves, and quasars and active galactic nuclei are among the most luminous sources of radiation in the universe.

A key aspect of galactic nuclei and SMBHs is that stars that wander too closely to the black hole can be captured or "tidally disrupted" by it. This process can occur by two ways: the star enters the event horizon (in the case of the most massive black holes), or the star gets tidally disrupted by the black hole if its pericenter is sufficiently close enough. Tidal disruption events (TDEs) can manifest themselves as a luminosity flare at the center of a galaxy for a few years [25], and the gas released from the disrupted star can be a source of power for quasars and AGN [12]. Much research has been done on the detection and spectra of these flares [18].

As tidally disrupted stars must have very small pericenter values, they occupy low angular momentum orbits in a galaxy. These orbits are called loss cone orbits, first coined by [10]. As the SMBH continuously empties the loss cone, these loss cone orbits must be repopulated by a relaxation in angular momentum. It is this loss cone repopulation mechanism that determines the rate of tidal disruption. The steady-state TDE rate in "typical" galaxies, where the loss cone repopulation is due to gravitational two body-relaxation processes, is of the order of $10^{-6} - 10^{-4}\ M_{\odot}\ \mathrm{yr}^{-1}$ [19, 29]. This rate prediction is consistent with the observed results.

However, black holes do not remain isolated forever. According to the standard Λ cold dark matter paradigm of structure formation in the universe, galaxies grow through the merger of smaller galaxies. We focus on the mergers of unequal mass galaxies. If both the merging galaxies contain an SMBH, then after an initial stripping away of stars, the two black holes will form a bound system. The dynamical evolution of supermassive black hole binaries (SMBHB) has been studied extensively [24, 22]. In the case of unequal mass binaries, the secondary (less massive) BH first inspirals towards the primary BH under the influence of dynamical friction, and then by binary hardening mechanisms (secondary slingshot and collisional loss cone repopulation). If the separation decreases to milliparsec scales, gravitational wave emission brings about their coalescence. The processes by which the binary can shrink to this separation is unclear, and this is known the final parsec problem.

Observing galaxy mergers and binary black hole evolution is itself a challenge. All galaxies are not active, and there are some nuclei with no or negligible surrounding disks, which are called inactive galaxies. The tidal disruption of stars is a promising phenomenon to observe these nuclei and make predictions of the capture rate of stars and evolution of supermassive black hole binaries.

We consider a hierarchical system of a primary black hole, a secondary black hole, and a star in a stellar cusp surrounding the primary. The star's otherwise Keplerian motion is affected by the presence of the secondary black hole, the gravity of the surrounding cluster, and general relativity. The combination of these effects results in a motion that is similar to the Lidov Kozai (LK) mechanism in celestial mechanics. The LK effect induces oscillations in the angular momentum l of the star, while conserving the l_z component. This greatly increases the loss cone feeding rate and capture by the SMBHB, resulting in a phase of enhanced capture rates. These rates

can reach up to $10^{-2} - 1\ M_\odot\ \mathrm{yr}^{-1}$, two to three orders of magnitude higher than the single black hole capture rate [13]. The enhancement due to a secondary BH has also been confirmed by N-body simulations [7, 17].

As the secondary black hole inspirals towards the primary, the dynamics of the stars of the cusp change. At large separations, apsidal precession due to the stellar potential greatly suppresses the LK mechanism, resulting in a TDE rate similar to that of a nucleus containing a single SMBH. At small (sub-parsec) separations, general relativity becomes an important factor, which can also destroy the LK oscillations. The LK mechanism is most effective in the region where where the stellar potential effects and GR effects cancel out, leading to the enhanced phase. The duration of this phase is short, of the order of 10^6 yr. Therefore, an enhanced phase of tidal disruptions can be instrumental in the identification and study of galaxy mergers [4, 5].

This thesis is organized as follows. In chapter 2, we review the dynamic processes which govern the motion of a star in a nucleus containing a SMBHB. In chapter 3, we combine these effects and present a hybrid model that combines the stellar potential, GR, and Lidov-Kozai mechanism. Using these dynamics we calculate the capture rates as a function of binary separation and input parameters. We derive analytic expressions for the peak rate and the duration of enhancement. In chapter 4, we present the results of our model and explore the input parameter space. We compare our results to existing N-body simulations. We conclude in chapter 5. The structure of our calculations is illustrated in figure 1

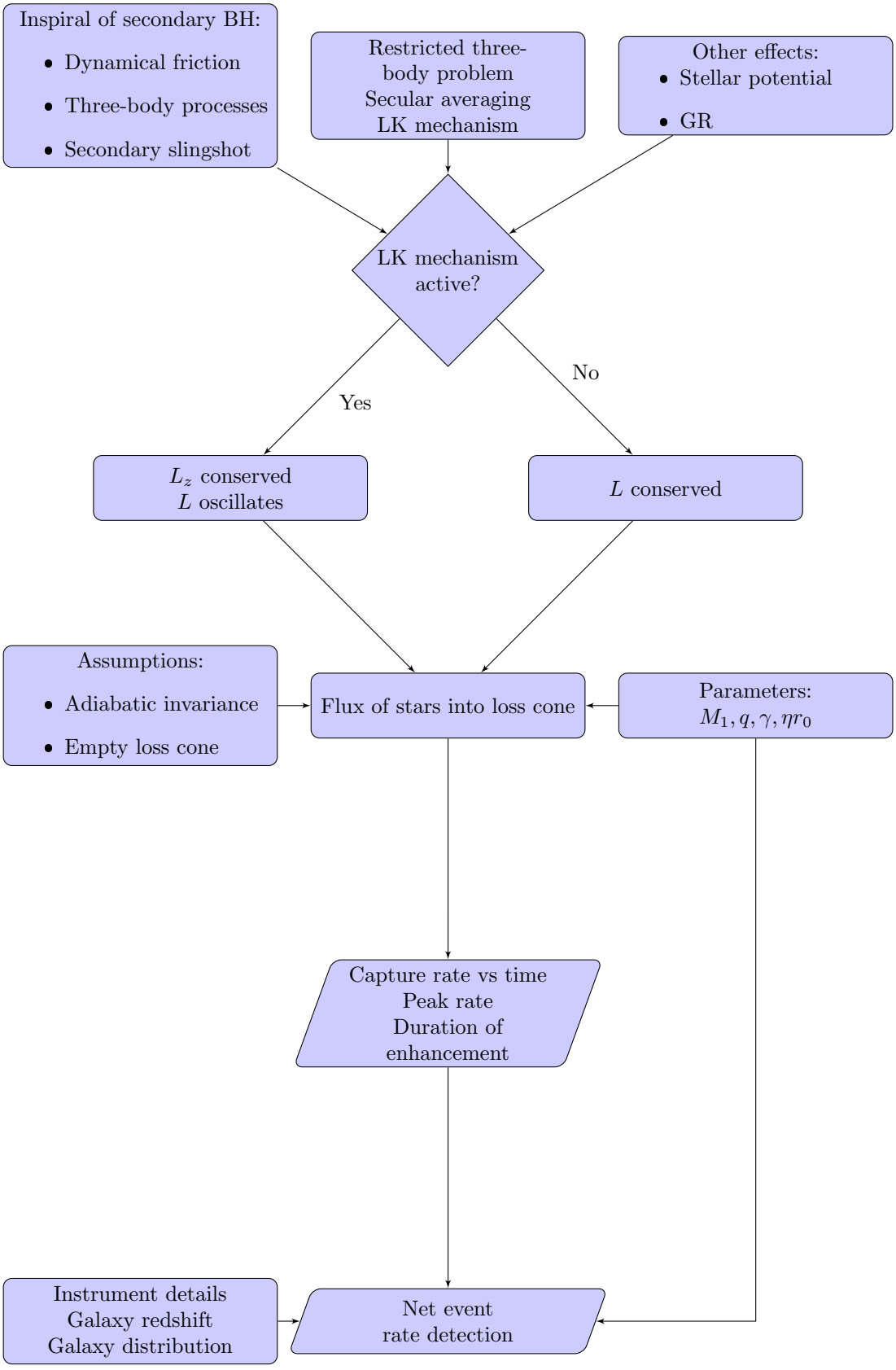

Figure 1.1: The flowchart we follow for the calculating the stellar capture rate

Chapter 2

Orbital Mechanics around Supermassive Black Holes

2.1 Stellar Dynamics

2.1.1 Hamiltonian Framework

The Hamiltonian for a particle moving under a central potential $U(r)$ in spherical coordinates is given by

$$H = T + V = \frac{1}{2}m^2 + U(r) = \frac{1}{2}m(\dot{r}^2 + r^2\dot{\theta}^2 + r^2\sin^2\theta\dot{\phi}^2) + U(r)\ . \tag{2.1}$$

The conjugate momenta are:

$$p_r = m\dot{r}\ , \tag{2.2a}$$
$$p_\theta = mr^2\dot{\theta}\ , \tag{2.2b}$$
$$p_\phi = mr^2\sin^2\theta\dot{\phi}\ . \tag{2.2c}$$

Substituting in equation 2.1, we have

$$H = \frac{1}{2m}\left(p_r^2 + \frac{p_\theta^2}{r^2} + \frac{p_\phi^2}{r^2\sin^2\theta}\right) + U(r)\ . \tag{2.3}$$

Since the Hamiltonian does not explicitly depend on time, we can use the Hamilton-Jacobi equation to obtain the characteristic function. Separating the variables r, θ, and ϕ, the characteristic function will be of the form

$$W = W_r(r) + W_\theta(\theta) + W_\phi(\phi)\ . \tag{2.4}$$

Since H is cyclic in the ϕ coordinate, the corresponding conjugate momentum is conserved

$$p_\phi = \alpha_\phi = \frac{\partial W_\phi}{\partial\phi} \implies W_\phi = \alpha_\phi\phi\ . \tag{2.5}$$

Substituting $p_r = \frac{\partial W_r}{\partial r}$ and $p_\theta = \frac{\partial W_\theta}{\partial\theta}$ in equation 2.3, we have

$$\frac{1}{2m}\left(\left(\frac{\partial W_r}{\partial r}\right)^2 + \frac{1}{r^2}\left[\left(\frac{\partial W_\theta}{\partial\theta}\right)^2 + \frac{\alpha_\phi^2}{sin^2\theta}\right] + U(r)\right) = H\ , \tag{2.6}$$

$$\left(\frac{\partial W_r}{\partial r}\right)^2 + \frac{1}{r^2}\left[\left(\frac{\partial W_\theta}{\partial\theta}\right)^2 + \frac{a_\phi^2}{sin^2\theta}\right] + 2mU(r) = 2mE\ , \tag{2.7}$$

where we substituted H with the total energy E, as the Hamiltonian is time-independent.
The quantity inside the square brackets of equation 2.7 only depends on θ, and the rest of the RHS depends only on r. Together, they give a constant $2mE$. Thus, the quantity in the square brackets must be a constant:

$$\left(\frac{\partial W_\theta}{\partial \theta}\right)^2 + \frac{\alpha_\phi^2}{sin^2\theta} = \alpha_\theta^2 \ . \tag{2.8}$$

The Hamiltonian thus becomes

$$H = \frac{1}{2m}\left(p_r^2 + \frac{\alpha_\theta^2}{r^2}\right) + U(r) \ ,$$

which reveals that $\alpha_\theta = l$, the magnitude of the total angular momentum.
Substituting for p_r and H, we find 2.7,

$$\left(\frac{\partial W_r}{\partial r}\right)^2 + \frac{\alpha_\theta^2}{r^2} = 2m(E - U(r)) \ ,$$

$$W_r = \int \sqrt{2m(E - U(r)) - \frac{\alpha_\theta^2}{r^2}}\, dr \ . \tag{2.9}$$

Now, we substitute for the gravitational potential $U(r) = -\frac{k}{r}$. This will allow us to generate the three pairs of action-angle variables for the problem.

$$J_\phi = \oint \frac{\partial W_\phi}{\partial \phi} d\phi = \oint \alpha_\phi d\phi = 2\pi\alpha_\phi \ , \tag{2.10}$$

$$J_\theta = \oint \frac{\partial W_\theta}{\partial \theta} d\theta = \oint \sqrt{\alpha_\theta^2 - \frac{\alpha_\phi^2}{sin^2\theta}}\, d\theta = 2\pi(\alpha_\theta - \alpha_\phi) \ , \tag{2.11}$$

$$J_r = \oint \frac{\partial W_r}{\partial r} = \oint \sqrt{2m(E + \frac{k}{r}) - \frac{a_\theta^2}{r^2}}\, dr = -(J_\theta + J_\phi) + \pi k\sqrt{\frac{2m}{-E}} \ . \tag{2.12}$$

Equation 2.12 can be inverted to get

$$E = -\frac{2\pi^2 m k^2}{(J_r + J_\theta + J_\phi)^2} \ . \tag{2.13}$$

We see that all of the action variables occur together, in the form $J_r + J_\theta + J_\phi$, which implies that the motion is completely degenerate [11]. There is only one frequency of motion:

$$\nu_r = \nu_\theta = \nu_\phi = \frac{\partial J_r}{\partial r} = \frac{\partial J_\theta}{\partial \theta} = \frac{\partial J_\phi}{\partial \phi} = \frac{4\pi^2 m k^2}{(J_r + J_\theta + J_\phi)^3} \ . \tag{2.14}$$

Substituting for $J_r + J_\theta + J_\phi$,

$$\nu = \frac{1}{\pi k}\sqrt{\frac{-2E^3}{m}} \Rightarrow \tau = \pi k\sqrt{\frac{m}{-2E^3}} \ , \tag{2.15}$$

which is just the Keplerian frequency of an orbit.

2.1.2 Delaunay Variables

We define new action variables by taking linear combinations of the old variables [11]:

$$\begin{aligned} J_1 &= J_\phi \ , \\ J_2 &= J_\theta + J_\phi \ , \\ J_3 &= J_r + J_\theta + J_\phi \ . \end{aligned}$$

The corresponding angle variables ω_1 and ω_2 are constant. In addition, as p_θ, p_ϕ, and E are constants, J_1, J_2, and J_3 are constants.
It is easy to see that $\frac{J_1}{J_2} = \frac{p_\phi}{p_\theta} = \cos i$, where i is the inclination of the orbit with respect to the ϕ plane.

The eccentricity and semimajor axis of a Keplerian orbit of total angular momentum L and energy E are given by

$$e = \sqrt{1 + \frac{2EL^2}{mk^2}} ,$$
$$a = \frac{-k}{2E} .$$

Substituting, we have

$$a = \frac{J_3^2}{4\pi^2 mk^2} , \tag{2.16}$$

$$e = \sqrt{1 - \left(\frac{J_2}{J_3}\right)^2} . \tag{2.17}$$

The angle variables are related as:

$$\omega_1 = \frac{\partial W}{\partial J_1} = \frac{\Omega}{2\pi} , \tag{2.18}$$

$$\omega_2 = \frac{\partial W}{\partial J_2} = \frac{\omega}{2\pi} , \tag{2.19}$$

where Ω and ω are the longitude of the ascending node and argument of pericenter respectively.
The final angle variable ω_3 is simply the frequency of the orbit ν as shown earlier. It is convenient to express this in terms of the mean anomaly M, which can be related to the time period T as

$$M = 2\pi \frac{t - T}{T} .$$

This allows to define a set of variables:

$$l = M \tag{2.20}$$
$$h = \Omega \tag{2.21}$$
$$g = \omega \tag{2.22}$$
$$L = \sqrt{ma} \tag{2.23}$$
$$H = \sqrt{ma(1 - e^2)} \cos i \tag{2.24}$$
$$G = \sqrt{ma(1 - e^2)} . \tag{2.25}$$

These are the Delaunay variables [27].

2.1.3 Lidov-Kozai Mechanism

The hierarchial three-body problem is a special case of the general three body problem in which the system consists of an inner binary which is perturbed by a distant object [27]. Consider three bodies of mass M_1, M_2, and m. Let $\mathbf{r}_1$ and $\mathbf{r}_2$ be the position vectors from M_1 to m and M_2, respectively. The equations of motion of these masses are:

$$\ddot{\mathbf{r}}_1 + G(M_1 + m)\frac{\mathbf{r_1}}{r_1^3} = GM_2 \left(\frac{\mathbf{r}_2 - \mathbf{r}_1}{|\mathbf{r}_2 - \mathbf{r}_1|^3} - \frac{\mathbf{r}_2}{r_2^3} \right) ,$$
$$\ddot{\mathbf{r}}_2 + G(M_1 + M_2)\frac{\mathbf{r_2}}{r_2^3} = Gm \left(\frac{\mathbf{r}_1 - \mathbf{r}_2}{|\mathbf{r}_1 - \mathbf{r}_2|^3} - \frac{\mathbf{r}_1}{r_1^3} \right) .$$

We want to investigate the motion of the mass m. The expression for $\ddot{\mathbf{r}}_1$ can be expressed in terms of the gradient of a scalar potential:

$$\ddot{\mathbf{r}}_1 = -\nabla_1(\Phi_1 + R_1) \tag{2.26}$$

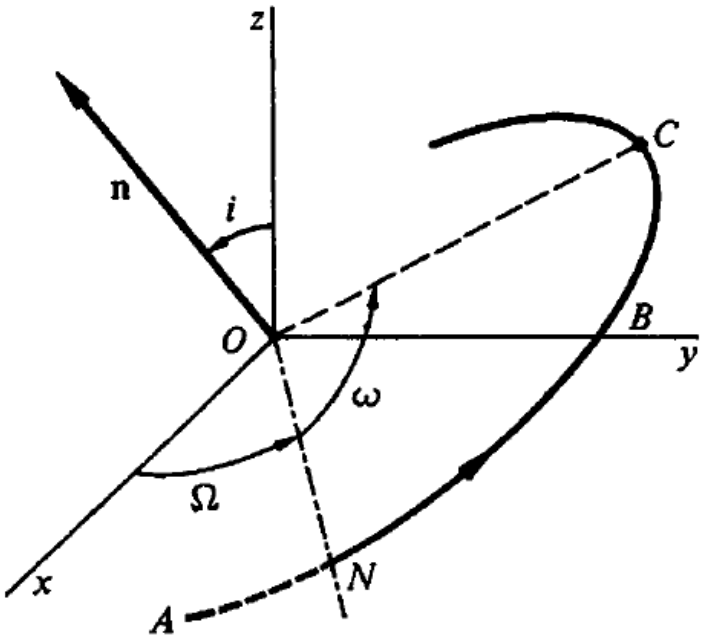

Figure 2.1: The Delaunay variables. C is the point of periapsis, and ON is the line of nodes. Figure taken from [11].

where $\Phi_1 = -G\frac{M_1+m}{r_1}$ is just the Keplerian part of the total potential, and

$$R_1 = -\frac{GM_2}{|\mathbf{r}_2 - \mathbf{r}_1|} + GM_2\frac{\mathbf{r}_1 \cdot \mathbf{r}_2}{r_2^3} \tag{2.27}$$

is called the disturbing function [27].
Assuming that $r_2 > r_1$, we can expand the denominator of the first term in terms of Legendre polynomials. Taking the angle between $\mathbf{r}_1$ and $\mathbf{r}_2$ as ϕ, we have

$$R_1 = -\frac{GM_2}{r_2}\sum_{l=0}^{\infty}\left(\frac{r_1}{r_2}\right)P_l(\cos\phi) + GM_2\frac{r_1}{r_2^2}\cos\phi\ . \tag{2.28}$$

Since the $l = 0$ term does not contain r_1, it does not contribute to the equation of motion of m. The $l = 1$ term of the expansion cancels the second term of R_1. So, the next lowest order contribution to the potential is at $l = 2$:

$$R_1 \approx -\frac{GM_2r_1^2}{r_2^3}\frac{3\cos^2\phi - 1}{2}$$

Furthermore, we make a change of variables to Jacobi coordinates:

$$\mathbf{r} = \mathbf{r}_1 \qquad \mathbf{r}' = \mathbf{r}_2 - \frac{m}{M_1+m}\mathbf{r}$$

In effect, this reduces the problem to an "inner binary" consisting of m and M_1, and an "outer binary" of M_2 which is orbiting the center of mass of the inner binary. We further define a new angle ψ as $\cos\psi = \frac{\mathbf{r}\cdot\mathbf{r}'}{rr'}$, the angle between $\mathbf{r}$ and $\mathbf{r}'$. In terms of the new variables, the disturbing function (to quadrupolar approximation) is

$$R_1 \approx -\frac{GM_2r^2}{r'^3}\frac{3\cos^2\psi - 1}{2}\ . \tag{2.29}$$

The corresponding Hamiltonian for the system is given by

$$H = H_{Kep} + H_p\ ,$$

where

$$H_{Kep} = -\frac{GM_1 m}{2a_1} - \frac{G(M_1+m)M_2}{2a_2} \tag{2.30}$$

is the Keplerian Hamiltonian with a_1 and a_2 being the two semimajor axes, and

$$H_P = -\frac{GM_1M_2m}{2(M_1+m)}\frac{r^2}{r'^3}(3\cos^2\psi - 1) \tag{2.31}$$

is the perturbing term due to the quadrupolar effect of the second body.
We now employ the technique of secular averaging to reduce the problem by two variables. The orbit average of any quantity $X(r)$ is given by [21]

$$\overline{X} = \frac{1}{2\pi}\int_0^{2\pi} dE(1 - e\cos E)X[a(1 - e\cos E)] \, .$$

As is evident, this procedure eliminates r from the quantity and replaces it with some combination of a and e, both of which are orbit elements. We want to eliminate both r and r', so we first average over the outer orbit, and then the inner orbit. The doubly averaged perturbing Hamiltonian is given by

$$\overline{\overline{H}}_P = \frac{GM_1M_2ma_1^2}{8(M_1+m)a_2^3(1-e_2^2)^{3/2}}\left[-2 - 3e_1^2 - 3\sin^2 i(5e_1^2\sin^2\omega_1 + 1 - e_1^2)\right] \, . \tag{2.32}$$

The details of the averaging are in [27].
The inner restricted problem makes the further approximation that $m << M_1, M_2$. The unsubscripted variables hereon will refer to the inner binary. We further simplify the expression by dividing by $m\nu_0 L_c$, where $\nu_0 = \frac{GM_2a^{3/2}}{\sqrt{GM_1a_2^3(1-e_2^2)^{3/2}}}$ and $L_c = \sqrt{GM_1a}$. This allows us to define a dimensionless Hamiltonian per unit mass of m [21]:

$$H = \frac{1}{8}\left[-5 + 3l^2 + 3\sin^2 i(l^2 + 5e^2\sin^2\omega)\right] \tag{2.33}$$

where $l = L/L_c$ is the dimensionless angular momentum and $\cos i = l_z/l$.
We immediately see that since the Hamiltonian is cyclic in Ω, the conjugate momentum l_z is conserved. The other equations of motion are:

$$\frac{d\omega}{d\tau} = \frac{\partial H}{\partial l} = \frac{3}{4l}\left[2l^2 + 5\sin^2\omega(e^2 - \sin^2 i)\right] \, , \tag{2.34}$$

$$\frac{dl}{d\tau} = -\frac{\partial H}{\partial \omega} = -\frac{15}{8}e^2\sin^2 i\sin(2\omega) \, , \tag{2.35}$$

$$\frac{d\Omega}{d\tau} = -\frac{\partial H}{\partial l_z} = \frac{3}{4}\frac{\cos i}{l}(l^2 + 5e^2\sin^2\omega) \, , \tag{2.36}$$

$$\frac{dl_z}{d\tau} = \frac{da}{d\tau} = 0 \, , \tag{2.37}$$

where $\tau = T_K = \nu_0^{-1} = \frac{\sqrt{M_1}}{\sqrt{GM_2}}\frac{a_2^3}{a^{3/2}}(1-e_2^2)^{3/2}$ is the timescale of the oscillations. The equations of motion allow for the oscillation of l while conserving l_z. This is known as the Lidov-Kozai mechanism [16, 14]. In addition to l_z, there is a second conserved quantity due to the conservation of energy:

$$Q = e^2(5\sin^2 i\sin^2\omega - 2) \, . \tag{2.38}$$

The orbits can be classified into two classes:

- Circulation in ω: These orbits have $\frac{d\omega}{d\tau} = 0$ at $\omega = 0, \pi$. They exhibit minimal variations in inclination and eccentricity.
- Libration in ω: These orbits have $\frac{d\omega}{d\tau} = 0$ at $\omega = \pm\frac{\pi}{2}$. They exhibit large oscillations in inclination and eccentricity, and are of more interest to us. The angular momentum can oscillate between $l \sim l_z$ to $l \sim 1$.

Librating orbits require the existence of a fixed point at $\omega = \pm\frac{\pi}{2}$, at which

$$l^2 = l_{fp}^2 = \sqrt{5/3} l_z \ .$$

Since $l_{fp} \leq 1$, librating orbits exist only for $l_z \leq \sqrt{3/5} = 0.775$.
The maximum and minimum angular momenta (l_+ and l_- respectively) that are achieved during the orbit are related by

$$l_- l_+ = l_{fp}^2 \ . \tag{2.39}$$

The time period of these oscillations is given by [13]

$$P_K = \frac{2}{e_+ \sqrt{3(3e_-^2 + 2)}} K(y) T_K \tag{2.40}$$

where $K(y)$ is the complete elliptic integral of the first kind, e_+ and e_- are the maximum and minimum eccentricities reached during the oscillation, and

$$y = \sqrt{\frac{2(1 - e_-^2/e_+^2)}{3e_-^2 + 2}} \ . \tag{2.41}$$

The difference between P_k and T_k is small when there are no other modes of precession involved.

2.1.4 Competing Mechanisms

2.1.4.1 Stellar Potential Precession

A stellar cluster around a SMBH perturbs the orbit of a star from the regular Keplerian ellipse. We assume a spherical cluster, where the density of the nucleus is represented by

$$\rho = \rho_0 \left(\frac{r}{r_0}\right)^{-\gamma} \ . \tag{2.42}$$

The corresponding potential is [21]

$$\Phi_s(r) = \begin{cases} \frac{4\pi}{(2-\gamma)(3-\gamma)} G\rho_0 r_0^2 \left(\frac{r}{r_0}\right)^{2-\gamma} & \gamma \neq 2 \\ 4\pi G \rho_0 r_0^2 \log\left(\frac{r}{r_0}\right) & \gamma = 2 \ . \end{cases} \tag{2.43}$$

Assuming that the frequency of precession is much lesser than the unperturbed Keplerian frequency, we can employ the technique of averaging to analyze the motion. The orbit-averaged potential is

$$\overline{\Phi}_P = \frac{1}{2\pi} \int_0^{2\pi} dE (1 - e\cos E) \Phi_s(a(1 - e\cos E)) \ . \tag{2.44}$$

The precession rate is the rate of change of the Delaunay variable ω, which can be calculated by Hamilton's equations

$$\frac{d\omega}{dt} = \frac{\partial \overline{\Phi}_P}{\partial L} = -\frac{1}{L_c} \frac{\sqrt{1-e^2}}{e} \frac{\partial \overline{\Phi}_P}{\partial e} \ . \tag{2.45}$$

Substituting for the stellar potential 2.43 into 2.44 and then the orbit-averaged potential into Hamilton's equations, we have [21]:

$$\frac{d\omega}{dt} = -\nu G_M(e,\gamma) \sqrt{1-e^2} \left[\frac{M_*(a)}{M_1}\right] \ . \tag{2.46}$$

where $\nu = \frac{\sqrt{GM_1}}{a^{3/2}}$ is the unperturbed Kepler frequency, $M_*(a)$ is the mass of stars within a sphere of radius a, and $G_M(e,\gamma)$ is a numerical factor of order unity that weakly depends on e and γ.
It is important to note that the precession due to the stellar potential is retrograde (opposite to the direction of orbit circulation), as opposed to the precession in the Lidov-Kozai mechanism. The precession rate is proportional

to the angular momentum $L \propto \sqrt{1-e^2}$. It also increases with increase in a (due to increase in $M_*(a)$), so its effects are more significant for orbits outside the radius of influence of M_1.

2.1.4.2 General Relativity

General relativity effects of a Schwarzschild black hole induce precession of the pericenter of a stellar orbit. A complete revolution around the SMBH causes an angular change in pericenter given by [21] (to first order in v^2/c^2)

$$\Delta\phi = \frac{6\pi GM}{a(1-e^2)c^2} \,, \tag{2.47}$$

where $M = M_1 + m \approx M_1$. The orbit-averaged precession rate is

$$\frac{d\omega}{dt} = \frac{\nu}{2\pi}\Delta\phi = \frac{3(GM)^{3/2}}{a^{5/2}(1-e^2)c^2} \,. \tag{2.48}$$

The GR precession is prograde (in the same direction as the orbit circulation), and it is proportional to $L^{-2} \propto \frac{1}{1-e^2}$. Unlike stellar potential precession, GR precession increases with decrease in a, so its effects are more significant very close to the black hole, i.e. in the sub-parsec scales.

2.2 Loss Cone Dynamics

2.2.1 Introduction

A star that wanders too close to a black hole can get tidally disrupted due to the intense gravitational pull of the black hole [9]. The condition for tidal disruption is that the tidal force of the black hole is greater than the star's self-gravity. For a star of mass M_* and radius R_* at a distance r from a SMBH of mass M, we have

$$\eta^2 \frac{GMr_*}{r^3} = \frac{Gm_*}{r_*^2}$$

where η is a parameter of order unity which depends on the polytropic index of the star. The tidal radius is thus given by [19]

$$r_t = \left(\eta^2 \frac{M}{m_*}\right)^{1/3} r_* \,.$$

If $r_t > r_g$, the event horizon radius of the BH, then an observable tidal disruption event (TDE) is produced. On the other hand, if $r_t < r_g$, the star is swallowed whole into the BH without a TDE flare. For solar mass stars, this happens if $M > 10^8 M_*$. We define captures to include both cases in order to derive a general formula for capture rate into the BH.

An orbit with a periapsis of r_t has angular momentum equal to $L_{lc} = \sqrt{2r_t^2(E-\Phi(r_t))} \approx \sqrt{2GMr_t}$ (we assume that the orbit is highly eccentric). Orbits with $L \leq L_{lc}$ are called loss cone orbits, and the set of all loss cone orbits is called the loss cone.

Loss cone orbits need to be repopulated as the stars get captured into the BH, i.e. they require some mechanism of loss cone repopulation. The flux of stars into the loss cone is determined by this mechanism, and can be calculated by solving the Fokker-Planck equation.

2.2.2 Spherical Nuclei

We define $\mathcal{E} = -E = -v^2/2 - \Phi(r)$ and $\mathcal{R} = L^2/L_c^2$.

The orbit-averaged Fokker-Planck equation in $(\mathcal{E}, \mathcal{R})$ coordinates is [21]

$$\frac{\partial N}{\partial t} = -\frac{\partial}{\partial \mathcal{E}}(N\langle\Delta\mathcal{E}\rangle) + \frac{1}{2}\frac{\partial^2}{\partial \mathcal{E}^2}(N\langle(\Delta\mathcal{E})^2\rangle) - \frac{\partial}{\partial \mathcal{R}}(N\langle\Delta\mathcal{R}\rangle) + \frac{1}{2}\frac{\partial^2}{\partial \mathcal{R}^2}(N\langle(\Delta\mathcal{R})^2\rangle) + \frac{\partial^2}{\partial \mathcal{E}\mathcal{R}}(N\langle(\Delta\mathcal{E})(\Delta\mathcal{R})\rangle) \,. \tag{2.49}$$

For efficient repopulation of the loss cone orbits, we require that the timescale of change in angular momentum is much smaller than the timescale of change in energy [21]. Therefore over an angular momentum timescale, we

can ignore the energy changes in the Fokker Planck equation [21]

$$\frac{\partial N}{\partial t} = -\frac{\partial}{\partial \mathcal{R}}(N\langle \Delta\mathcal{R}\rangle) + \frac{1}{2}\frac{\partial^2}{\partial \mathcal{R}^2}(N\langle(\Delta\mathcal{R})^2\rangle) \ . \tag{2.50}$$

The two angular-momentum diffusion coefficients are related by (to first order approximation) [21]

$$\langle \Delta\mathcal{R}\rangle = \frac{1}{2}\frac{\partial}{\partial \mathcal{R}}\langle(\Delta\mathcal{R})^2\rangle \ . \tag{2.51}$$

We define

$$\mathcal{D}(\mathcal{E}) = \lim_{\mathcal{R}\to 0}\frac{\langle(\Delta\mathcal{R})^2\rangle}{2\mathcal{R}} \tag{2.52}$$

which scales inversely with the angular momentum relaxation time.
The Fokker-Planck equation 2.50 then becomes

$$\frac{\partial N}{\partial t} = \mathcal{D}\frac{\partial}{\partial \mathcal{R}}\left(\mathcal{R}\frac{\partial N}{\partial \mathcal{R}}\right) \ . \tag{2.53}$$

The above equation can be expressed just as well in terms of f, the distribution function. We perform another change of variables to $y = \frac{\mathcal{R}}{P\mathcal{D}}$, where $P = P(\mathcal{E})$ is the radial period of the orbit. In terms of y and the timelike variable $\tau = (P\mathcal{D})^{-1}\int_{r_-}^{r_+}\frac{dr}{\nu_r}\frac{\langle(\Delta\mathcal{R})^2\rangle}{2\mathcal{R}}$, we have [21]

$$\frac{\partial f}{\partial \tau} = \frac{\partial}{\partial y}\left(y\frac{\partial f}{\partial y}\right) \tag{2.54}$$

which is equivalent to the equation of radial heat transfer in a cylinder.
The boundary conditions are [21]

$$f(0,y) = f(1,y) \quad \text{for } y > y_{lc} \qquad \text{(steady state)} \tag{2.55}$$

$$f(0,y) = 0 \quad \text{for } y < y_{lc} \qquad \text{(capture into the BH)} \tag{2.56}$$

$$\frac{\partial f}{\partial L} \propto \frac{\partial f}{\partial \sqrt{y}} = 0 \quad \text{at } y = 0 \qquad \text{(smoothness of f)} \tag{2.57}$$

The solution equation 2.54, satisfying the boundary conditions 2.55-2.57, is [21]

$$f(\tau,y) = f(y_{lc})\left[1 - \frac{2}{\sqrt{y_{lc}}}\sum_{m=1}^{\infty}\frac{e^{-\beta_m^2\tau/4}}{\beta_m}\frac{J_0(\beta_m\sqrt{y})}{J_1(\beta_m\sqrt{y_{lc}})}\right] \ , \tag{2.58}$$

where J_0 and J_1 are Bessel functions of the first kind, and β_m yield consecutive zeros of the equation $J_0(\beta\sqrt{y_{lc}}) = 0$.
In spherical geometry, the number of stars per unity energy per unity angular momentum is related to the distribution function as

$$N(\mathcal{E},\mathcal{R})d\mathcal{E}d\mathcal{R} = 4\pi^2 P(\mathcal{E})L_c^2(\mathcal{E})f(\mathcal{E},\mathcal{R})d\mathcal{E}d\mathcal{R} \ . \tag{2.59}$$

The flux of stars per unit energy into the BH is then given by integrating equation 2.59 over $\mathcal{R}$ and dividing by the relaxation time:

$$F(\mathcal{E})d\mathcal{E} = \frac{N_{lc}}{\tau_{relax}} = 4\pi^2 P(\mathcal{E})D(\mathcal{E})L_c^2(\mathcal{E})\left[\int_0^{y_{lc}} f(1,y)dy\right]d\mathcal{E} \ . \tag{2.60}$$

On substituting for f and integrating, we have

$$F(\mathcal{E}) = 4\pi^2 L_c^2\mathcal{R}_{lc}f(\mathcal{R}_{lc})\left(1 - 4\sum_{m=1}^{\infty}\frac{e^{\alpha_m^2 q/4}}{\alpha_m^2}\right) = 4\pi^2 L_c^2\mathcal{R}_{lc}f(\mathcal{R}_{lc})\xi(q) \ , \tag{2.61}$$

where α_m are the consecutive zeros of the Bessel function $J_0(\alpha)$ and $q = \frac{P(\mathcal{E})\mathcal{D}(\mathcal{E})}{\mathcal{R}_{lc}(\mathcal{E})}$.
The value of $f(\mathcal{R}_{lc})$ is determined from matching the boundary conditions, particularly, the steady state condition

2.55 and smoothness condition 2.57:

$$f(\mathcal{R}) = f(\mathcal{R}_{lc}) + \frac{f(1) - f(\mathcal{R}_{lc})}{\ln(1/\mathcal{R}_{lc})} \ln(\mathcal{R}/\mathcal{R}_{lc}) \ , \tag{2.62}$$

which implies a flux of

$$F(\mathcal{E}) = 4\pi^2 L_c^2 P \mathcal{D} \mathcal{R}_{lc} \frac{\partial f}{\partial \mathcal{R}} |_{\mathcal{R}_{lc}} \ . \tag{2.63}$$

Equating the two expressions 2.61 and 2.63 at $\mathcal{R}_{lc}$, we have

$$f(\mathcal{R}_{lc}) = \frac{f(1)}{1 + q^{-1}\xi(q)\ln(1/\mathcal{R}_{lc})} \ . \tag{2.64}$$

Substituting in equation 2.61, we have

$$F(\mathcal{E}) = 4\pi^2 L_c^2 \mathcal{R}_{lc} \frac{\overline{f}(\mathcal{E})}{\xi(q)^{-1} + q^{-1}\ln(1/\mathcal{R}_{lc})} \ , \tag{2.65}$$

where we have approximated $\overline{f}(E) \approx f(1)$, the average of the distribution function over angular momenta. Equation 2.65 can be written concisely as

$$F(\mathcal{E}) = 4\pi^2 q L_{lc}^2 \frac{\overline{f}(\mathcal{E})}{\ln(1/\mathcal{R}_0)} \ , \tag{2.66}$$

where $\mathcal{R}_0(q) = \mathcal{R}_{lc} e^{-q/\xi(q)}$. A numerical approximation to $\xi(q)$ is given by [18]

$$\xi(q) = \begin{cases} 1 & q \geq 4 \\ \frac{q}{0.86q^{0.5} + 0.384q - 0.379q^{1.5} + 0.427q^2 - 0.095q^{2.5}} & q < 4 \end{cases} \ . \tag{2.67}$$

The quantity q is the ratio of the time period and the time taken to diffuse across the loss cone. The limit $q << 1$ is the diffusive or empty loss cone, where a star may wander in and out of the loss cone many times before capture. On the other hand, $q >> 1$ is the pinhole or full loss cone, where a star is captured in a single orbital period.

2.2.3 Axisymmetric Nuclei

The general motion in an axisymmetric potential allows for three integrals of motion: the energy E, the z-component of the angular momentum L_z, and a third integral (which is generally taken to be the total angular momentum L). There are two classes of orbits: saucers (similar to librating orbits in the LK mechanism) and tubes (similar to circulating orbits) [21]. Assuming a weak dependence on the third integral, the number density of stars $N(E, L_z)$ is related to the distribution function $f(E, L_z)$ by [21]

$$N(E, L_z) dE dL_z = 4\pi^2 P(E) L_{sep} f(E, L_z) dE dL_z \ , \tag{2.68}$$

where L_{sep} is the separatrix between saucer and tube orbits and P(E) is the time period of radial motion. The flux into the loss cone is given by [21]

$$F(E)dE = -\frac{d}{dt}\left[\int_{L_{lc}}^{L_{sep}} dL_z N(E, L_z)\right] dE \ . \tag{2.69}$$

The axisymmetric Fokker-Plank equation in $\mathcal{E}$, L_z variables is [21]

$$\frac{\partial N}{\partial t} = -\frac{\partial}{\partial \mathcal{E}}(N\langle \Delta\mathcal{E}\rangle) + \frac{1}{2}\frac{\partial^2}{\partial \mathcal{E}^2}(N\langle(\Delta\mathcal{E})^2\rangle) - \frac{\partial}{\partial L_z}(N\langle \Delta L_z\rangle) + \frac{1}{2}\frac{\partial^2}{\partial L_z^2}(N\langle(\Delta L_z^2\rangle) + \frac{\partial^2}{\partial \mathcal{E} L_z}(N\langle(\Delta\mathcal{E})(\Delta L_z)\rangle) \ . \tag{2.70}$$

We again consider changes in L_z to be the dominant relaxation mechanism. From the above equation, we can relate the flux and the diffusion coefficients [21]:

$$\frac{\partial N}{\partial t} = \frac{1}{2}\frac{\partial^2}{\partial L_z^2}\left(\langle(\Delta L_z)^2\rangle\right) \approx \frac{\mathcal{D}L_c^2}{8}\frac{\partial^2 N}{\partial L_z^2} \ . \tag{2.71}$$

Here as before, the diffusion coefficient $\mathcal{D}$ is related to τ, the time taken for L to change by order L_c:

$$\mathcal{D} = \frac{\mathcal{R}_{lc}}{\tau} \ . \tag{2.72}$$

Substituting this in equation 2.69, we get

$$F(E)dE \approx \frac{\pi^2}{8}\mathcal{D}L_c^2\left[\left(\frac{\partial N}{\partial L_z}\right)_{L_{lc}}\right]dE = \frac{\pi^2}{2}\mathcal{D}P(E)L_c^2 L_{sep}\frac{\partial f}{\partial L_z}dE \ . \tag{2.73}$$

A similar result is derived in MT99, except for a factor of 2π instead of $\pi^2/2$.
The flux into the loss cone can by computed by arguing that in a steady state galaxy, the flux must be independent of L_z. Therefore, f must be linear in L_z, i.e. $f(E, L_z) = a(E) + b(E)|L_z|$.
The functions $a(E)$ and $b(E)$ can be found by employing the pinhole and diffusive loss cone limits on $f(E, L_z)$, as is done in [19]. The solution is

$$f(E, L_z) = \overline{f}(E)\frac{1 + 2\pi|L_z|/qL_{sep}}{1 + \pi L_c/qL_{sep}} \ , \tag{2.74}$$

where $q = P/\tau = P\mathcal{D}/\mathcal{R}_{lc}$ is a dimensionless variable and $\overline{f}(E)$ is the average of $f(E, L_z)$ over L_z. The empty loss cone (diffusion) regime is given by $q << 1$, and the full loss cone (pinhole) regime is given by $q >> 1$. The transition between empty and full loss cones takes place at $q \approx 4L_c/L_{sep}$. In most galactic nuclei containing a binary black hole, we will be in the diffusive region [22].
The flux into the loss cone is

$$F(E)dE = 4\pi^2 L_{lc}^2\frac{\overline{f}(E)}{1 + \pi L_c/qL_{sep}}dE \ . \tag{2.75}$$

This can be put into a more elegant form [28]:

$$F(E) = \frac{\mathcal{D}\overline{N}(E)}{q + \pi L_c/L_{sep}} \ . \tag{2.76}$$

2.3 Massive Binary Black Hole Evolution

The evolution of a binary black hole system can be categorized into three stages [20]:

- Stage 1: Inspiral due to dynamical friction
- Stage 2: Formation of hard binary by ejection of stars
- Stage 3: Continued hardening by secondary slingshot and collisional loss cone repopulation

2.3.1 Dynamical Friction

The Chandrasekhar dynamical friction formula for the change in velocity of an object of mass M as it falls through a field of stars of mass m and velocity distribution function $f(v)$ is [2]

$$\frac{d\mathbf{v}_M}{dt} = -16\pi^2 \ln\Lambda G^2 m(M + m)\frac{1}{v_M^3}\int_0^{v_M} v^2 f(v)dv\mathbf{v}_M \ , \tag{2.77}$$

where $\mathbf{v}_M$ is the velocity of the object under consideration and $\ln\Lambda$ is the Coulomb logarithm.
We consider that the secondary BH M_2 is inspirling into the primary BH M_1, while maintaining a nearly circular

orbit. This is a reasonable assumption because dynamical friction tends to circularize orbits. As before, we assume a stellar density distribution which varies as $\rho = \rho_0(r/r_0)^{-\gamma}$. If we assume that the inspiral time is long compared to the stellar orbital periods, we can apply the technique of orbit averaging to obtain an expression for the radius of M_2 as a function of time [21]:

$$\frac{dr}{dt} = -\sqrt{\frac{GM_1}{r_0}}\frac{M_2}{M_1}\ln\Lambda\left(\frac{r}{r_0}\right)^{\gamma/2-2} F(\gamma)\ , \tag{2.78}$$

where $F(\gamma)$ is a numerical factor of order unity.
At the onset of a galaxy merger, the binary separation is of the order of 10^2 *pc*. Dynamical friction brings down the separation to $\sim r_h$, the radius of influence of M_1, on a timescale of a few Gyr. N-body simulations and theoretical estimates show that when the binary separation comes down to $\sim r_h$, dynamical friction is no longer effective. In our model, we end the dynamical friction phase when $r = r_h$.

2.3.2 Formation of a Hard Binary

When stars interact with a massive binary, they tend to gain energy and are scattered onto new orbits, or even escape the system completely. This mechanism is called the gravitational slingshot. Stars gaining energy from this mechanism implies that the binary loses energy, and thus the separation decreases. This is the driving force behind stage 2 in MBHB evolution.
In our model, we consider an unequal mass binary with $M_2 << M_1$ as before. Since the primary BH is much more massive than either the field star or the secondary BH, most of the star's energy will come from interaction with M_2.The gravitational field of the M_2 is given by $F \approx GM_2/a^2$ and this acts approximately for a time $\Delta t = (a^3/GM_1)^{1/2}$ (Keplerian time period). Therefore, velocity changes by

$$\Delta v = F\Delta t = \frac{M_2}{M_1}V_{bin}\ , \tag{2.79}$$

where $V_{bin} = \sqrt{\frac{GM_1}{a}}$ is the circular binary velocity. The corresponding specific energy change is

$$\Delta E = \frac{1}{2}\left[(V+\Delta v)^2 - V^2\right] \approx V\cdot\Delta v = (M_2/M_1)V_{bin}^2\ . \tag{2.80}$$

The star's energy is increased at the expense of the binary's energy. Therefore, the binary's energy changes by

$$\Delta E_{bin} = -m_*\Delta E = -\frac{m_* M_2}{M_1}V_{bin}^2\ ,$$

or, a relative energy change of

$$\frac{\Delta E_{bin}}{E_{bin}} = -2\frac{m_*}{M_1}\ . \tag{2.81}$$

A decrease in energy (increase in negative energy) leads to a decrease in semimajor axis.
This expression must be averaged over all the orientations and initial phases of the binary, as well as the field star velocity distribution. As a result of the averaging, we define the binary hardening rate [21]:

$$\mathcal{H} = \frac{\sigma}{G\rho}\frac{d}{dt}\left(\frac{1}{a}\right)\ . \tag{2.82}$$

Simulations show that H can be expressed as $\mathcal{H} \approx q\mathcal{H}_\infty$ when $a \le r_h$, where $\mathcal{H}_\infty \approx 16$.
Phase 2 of the SMBHB ends when the binary separation reaches $\Delta r = a_h$, the hardening radius [21]

$$a_h = \frac{\mu}{M_{12}}\frac{r_h}{4} = \frac{q}{(1+q)^2}\frac{r_h}{4}\ . \tag{2.83}$$

The timescale associated with phase 2 evolution is of the order of $10^5 - 10^6$ yr.

2.3.3 Ssecondary Slingshot and Collisional Loss Cone Repopulation

In the case of hard binaries with $\Delta r \leq a_h$, the binary evolves with slingshot mechanism interactions with the field stars, as in phase 2. However, at such small separations, the fraction of stars which interact with the binary are ejected or lost from the system is much greater. As a result, there is a requirement of loss cone repopulation in order to maintain a supply of field stars, in order to facilitate the SMBHB evolution.

Let the semimajor axis of the binary be $a(t)$. A star which interacts strongly with the binary must have a pericenter distance of $r = Ka(t)$ where $1 \leq K \leq 2$. As in the single black hole case, we can define a loss cone angular momentum as

$$L_{lc}(\mathcal{E}, t) = Ka(t)\sqrt{2[\psi(Ka) - \mathcal{E}]} \approx \sqrt{2GM_{12}Ka(t)} \; . \tag{2.84}$$

It is important to note, however, that unlike the earlier case of capture, a star which enters into the loss cone is not necessarily "lost"; they interact with the binary strongly enough to contribute to its evolution.

N-body simulations show that the loss cone of a hard binary is in the pinhole regime, i.e. a full loss cone [23]. In this $q(\mathcal{E}) >> 1$ limit, the pinhole flux is given by

$$F(\mathcal{E})d\mathcal{E} = \frac{N(\mathcal{E})\mathcal{R}_{lc}(\mathcal{E})}{P(\mathcal{E})} d\mathcal{E} \; . \tag{2.85}$$

The above equation is valid for $\mathcal{E} < \mathcal{E}_{crit} \approx 9\sigma^2$.

The energy gained by the stars by this loss cone repopulation is compensated by the decrease in the binary's energy:

$$\frac{d}{dt}\left(\frac{GM_1M_2}{2a}\right) = -m_* \int \frac{N(\mathcal{E}, t)}{P(\mathcal{E})} \langle \Delta\mathcal{E} \rangle d\mathcal{E} \tag{2.86}$$

where $\langle \Delta\mathcal{E} \rangle$ is the average change in energy of the field stars per interaction. It is a reasonable approximation to assume that the change in energy of the stars is is of the order of their own kinetic energy:

$$\langle \Delta\mathcal{E} \rangle \sim v^2/2 = \frac{1}{2}\frac{GM_{12}}{a} \tag{2.87}$$

The evolution of the semimajor axis is then given by

$$\frac{d}{dt}\ln\frac{1}{a} = \frac{m_*}{M_1}\int_0^{\mathcal{E}_{crit}} F(\mathcal{E})d\mathcal{E} = \frac{\mathcal{D}}{2}\left(\frac{a}{a_h}\right)^2 \; , \tag{2.88}$$

where $\mathcal{D} = \frac{G^2 m_* \mu}{4\sigma^2}\int_0^{\mathcal{E}_{crit}} \frac{N(\mathcal{E})\langle\Delta\mathcal{E}\rangle}{P(\mathcal{E})L_c^2(\mathcal{E})} d\mathcal{E}$. Integration of the above equation gives

$$\frac{a_h}{a(t)} = \sqrt{1 + \mathcal{D}t} \tag{2.89}$$

which is a $\sqrt{t}$ dependence on the binary's binding energy [23].

In summary, the binary separation for the three stages in our model can be written as:

$$\begin{aligned}
\frac{dr}{dt} &= -\sqrt{\frac{GM_1}{r_0}}\frac{M_2}{M_1}\ln\Lambda\left(\frac{r}{r_0}\right)^{\gamma/2-2} F(\gamma) \qquad \text{for} \quad r > r_h \\
\frac{dr}{dt} &= -H\frac{G\rho r^2}{\sigma} \qquad \text{for} \quad r_h > r > a_h \\
\frac{a_h}{r(t)} &= \sqrt{1 + \mathcal{D}t} \qquad \text{for} \quad r < a_h
\end{aligned}$$

Chapter 3

Stellar Capture Rates in Supermassive Black Hole Binaries

3.1 Stellar Dynamics

Combining equations 2.34, 2.46, and 2.48 for the precession due to the LK mechanism, stellar potential, and general relativity respectively, we obtain an expression for the total precession rate:

$$\frac{d\omega}{dt} = \frac{1}{T_K}\frac{3}{4l}\left[2l^2 + 5\sin^2\ \omega(e^2 - \sin^2 \imath)\right] - \nu G_M(e,\gamma)\sqrt{1-e^2}\left[\frac{M_*(a)}{M_1}\right] + \frac{3(GM)^{3/2}}{a^{5/2}(1-e^2)c^2}\ , \tag{3.1}$$

$$\frac{d\omega}{d\tau} = \frac{3}{4l}\left[2l^2 + 5\sin^2\ \omega(e^2 - \sin^2 \imath)\right] - \kappa l + \frac{B}{l^2}\ , \tag{3.2}$$

where

$$\kappa = \nu G_M(e,\gamma)\left[\frac{M_*(a)}{M_1}\right] T_K$$

is a measure of the strength of the stellar potential, and

$$B = \frac{3(GM)^{3/2}}{a^{5/2}c^2} T_K$$

is a measure of the strength of GR.
The corresponding Hamiltonian is the integral of $\frac{d\omega}{d\tau}$ with respect to l:

$$H = \frac{1}{8}\left[-5 + 3l^2 + 3\sin^2 i(l^2 + 5e^2\sin^2\omega)\right] - \frac{\kappa l^2}{2} - \frac{B}{l}\ . \tag{3.3}$$

As the Hamiltonian in once again cyclic in Ω, l_z is conserved:

$$\Lambda = l_z = \sqrt{1-e^2}\cos i\ . \tag{3.4}$$

Using the constancy of the Hamiltonain , we obtain a second conserved quantity

$$H = \frac{1}{8}\left[-5 + 3(1-e^2) + 3\sin^2 i((1-e^2) + 5e^2\sin^2\omega)\right] - \frac{\kappa(1-e^2)}{2} - \frac{B}{\sqrt{1-e^2}} = \text{const}$$

$$1 - e^2 + \sin^2 i(1 - e^2 + 5e^2\sin^2\omega) - \frac{4\kappa(1-e^2)}{3} - \frac{8B}{3\sqrt{1-e^2}} = \text{const}$$

$$(2 - \cos^2 i)(1-e^2) + 5e^2\sin^2\omega\sin^2 i + \frac{4\kappa}{3}e^2 - \frac{8B}{3\sqrt{1-e^2}} = \text{const}$$

$$2(1-e^2) - (1-e^2)\cos^2 i + 5e^2\sin^2\omega\sin^2 i + \frac{4\kappa}{3}e^2 - \frac{8B}{3\sqrt{1-e^2}} = \text{const}$$

$$e^2\left(5\sin^2\omega\sin^2 i - 2 + \frac{4\kappa}{3}\right) - \frac{8B}{3\sqrt{1-e^2}} = \text{const} = Q\ .$$

It is convenient to visualize the oscillations in angular momentum using contour plots of constant Q in $\omega - l$ axes. We can see that at large binary separations ($D \lesssim 1$pc) the stellar potential precession destroys the Kozai oscillations, whereas for small separations ($D \gtrsim 0.05$pc) GR does the same. There seems to be a "sweet spot" where the two effects cancel out, allowing the Kozai effect to dominate.

We further proceed by eliminating i by $\sin^2 i = 1 - \frac{\Lambda^2}{1-e^2}$. For notational convenience, we redefine $4\kappa/3 \to \kappa$ and $8B/3 \to B$. Letting e_+ and e_- be the maximum and minimum eccentricities, we have

$$\sin^2 i_+ = 1 - \frac{\Lambda^2}{1-e_+^2}\ , \tag{3.5}$$

$$\sin^2 i_- = 1 - \frac{\Lambda^2}{1-e_-^2}\ . \tag{3.6}$$

Substituting these in the equation for Q, we have

$$Q = e_+^2\left(5\left(1 - \frac{\Lambda^2}{1-e_+^2}\right) - 2 + \kappa\right) - \frac{B}{\sqrt{1-e_+^2}} = e_-^2\left(5\left(1 - \frac{\Lambda^2}{1-e_-^2}\right) - 2 + \kappa\right) - \frac{B}{\sqrt{1-e_-^2}}\ . \tag{3.7}$$

Solving for Λ^2,

$$\Lambda^2 = \frac{3+k}{5}(1-e_+^2)(1-e_-^2) - \frac{B}{5}\left(\frac{\left(\sqrt{1-e_-^2} - \sqrt{1-e_+^2}\right)\sqrt{(1-e_+^2)(1-e_-^2)}}{e_+^2 - e_-^2}\right)\ . \tag{3.8}$$

Since this is one equation with two variables, we don't have a single solution for e_+ and e_-, rather we have a region of space in the e_+, e_- plane where the above equation is valid.

We also have the conditions

$$\sin^2 i_+ = 1 - \frac{\Lambda^2}{1-e_+^2} \geq 0\ , \tag{3.9}$$

$$\sin^2 i_- = 1 - \frac{\Lambda^2}{1-e_+^2} \leq 1\ . \tag{3.10}$$

Equation 3.8 is solved numerically, and the largest value of e_+ and the smallest value of e_-, which satisfy the two other conditions 3.9 and 3.10 as well, are taken into consideration. From the value of e_+ and e_-, we obtain the smallest and largest angular momenta attained during the Kozai cycle:

$$l_- = \sqrt{1-e_+^2} \qquad l_+ = \sqrt{1-e_-^2}\ . \tag{3.11}$$

However, sometimes the value of e_+ obtained from equation 3.8 may be such that $l_- < l_z$. This is physically impossible, as l_z is a conserved quantity during the oscillation and $l \geq l_z$. Therefore, we take

$$l_- = \max(l_z, \sqrt{1-e_+^2}) \qquad l_+ = \sqrt{1-e_-^2}\ . \tag{3.12}$$

For librating orbits to exist, we must have $l_+ > l_-$. In addition, librating orbits must have a fixed point in the $l - \omega$ space. Setting $\frac{d\omega}{d\tau} = 0$, we have

$$\frac{3}{4l}\left[2l^2 + 5\sin^2\ \omega(1 - l^2 - \sin^2\imath)\right] - \kappa l + \frac{B}{l^2} = 0\ . \tag{3.13}$$

The solution of this is l_{fp}, the fixed point angular momentum. For librating orbits to exist, we must have $0 < l_{fp} < 1$.

The size of the loss wedge also changes because of the torques exerted by the secondary. The effective loss wedge

size l_t is given by [13, 3]:

$$l_{lc} = l_t + \frac{15}{8}\sqrt{\frac{3}{5}} q \left(\frac{a}{D}\right)^{3/2} . \tag{3.14}$$

More details about the behavior of l_+, l_-, l_{lc}, and l_{fp} are given in Appendix A.

If $l_- \leq l_t$ in a saucer orbit, a star with angular monetum $\leq l_+$ can enter the loss cone and gets tidally disrupted. This is a considerably weaker restriction compared to the the condition $l \leq l_{lc}$. Therefore, the presence of the binary leads to a greater flux of stars into the loss cone compared to the isolated SMBH case.

A convenient way to visualize the orbits is through contour plots of constant Q in the $\omega - l$ plane. The strength of the Kozai effect is represented by the amplitude of oscillation in l over one libration cycle.

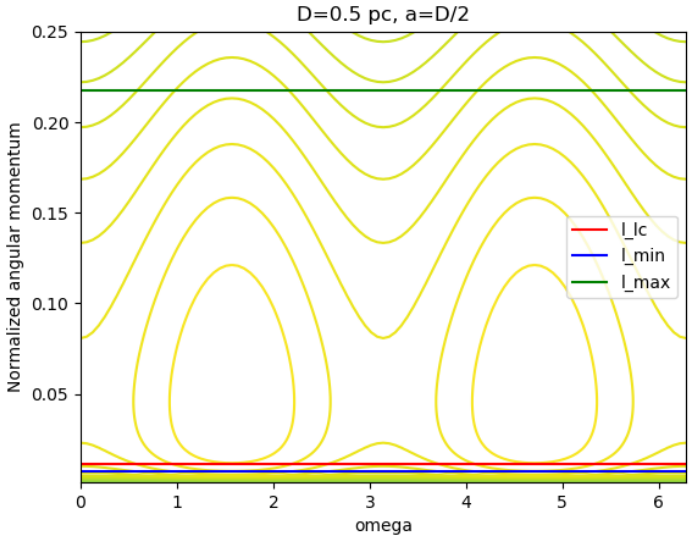

Figure 3.1: Contour plot of constant Q in the $\omega - l$ plane, for $D = 0.5$ pc, $a = D/2$. The parameters are $M_1 = 10^7 M_\odot$, $q = 0.01$, $\eta r_0 = 1$ pc, $\gamma = 1.5$. The angular momentum oscillates from ~ 0.01 to 0.22.

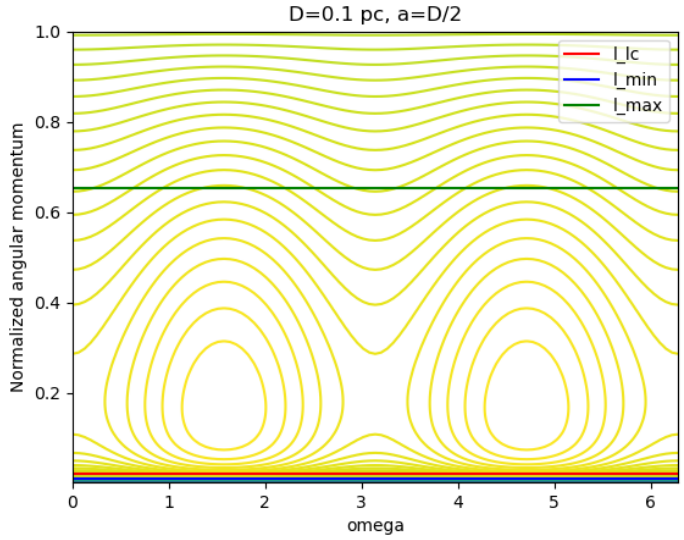

Figure 3.2: Similar plot as figure 3.1, at a binary separation of 0.1 pc. Note that the Kozai effect is much stronger, allowing a greater oscillation of l. Other parameters are the same as figure 3.1.

We also require the time period of these oscillations. Following [21], the time period can be expressed in

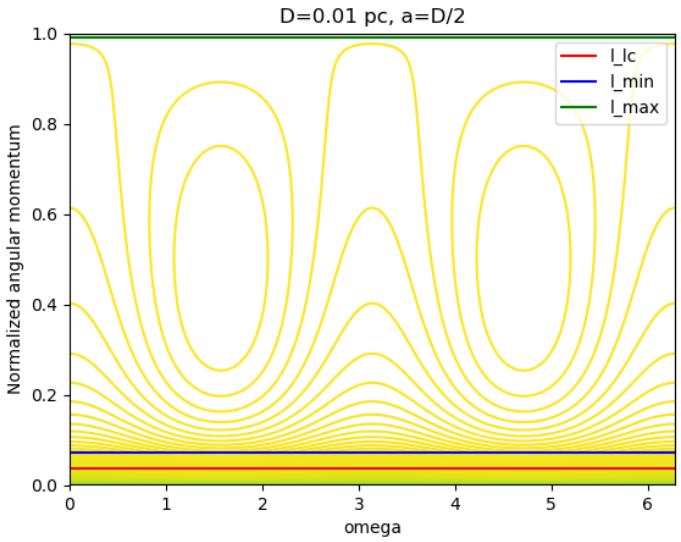

Figure 3.3: Similar plot as figure 3.1, at a binary separation of 0.01 pc. Due to GR effects, the value of l_{min} is greater than l_{lc}, so the Kozai oscillations cannot drive stars into the loss cone . Other parameters are the same as figure 3.1.

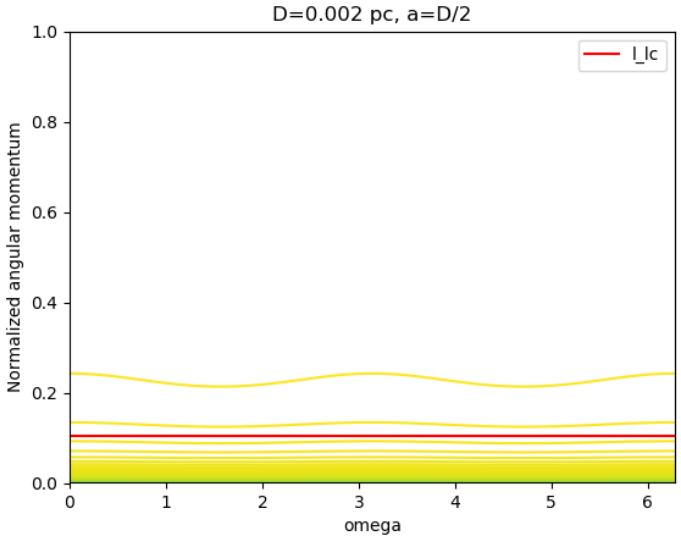

Figure 3.4: Similar plot as fig 3.1, at a binary separation of 0.002 pc. The Kozai oscillations are almost completely suppressed due to the strong GR effects. Other parameters are the same as figure 3.1.

terms of the minimum and maximum angular mometa reached during the cycle:

$$P_k = \frac{8}{3\sqrt{6}} \frac{K(k^2)}{\sqrt{z_1 - z_3}} T_k \ , \tag{3.15}$$

where,

$$\begin{aligned} z_1 &= 1 - l_-^2 \ , \\ z_2 &= 1 - l_+^2 \ , \\ z_3 &= -\frac{3}{2}(1 - l_+^2)\left(1 - \frac{l_{fp}^2}{l_+^2}\right) \ , \\ k^2 &= \frac{z_1 - z_2}{z_1 - z_3} \ , \end{aligned}$$

and $K(k^2)$ is the complete elliptic integral of the first kind with modulus k. The ratio P_K/T_K ranges from $\sim 1-10$.

3.2 Capture Rate

As we saw in section 2.1.3, the inner restricted three body problem conserves L_z and E while allowing L to oscillate. In essence, the dynamics are similar to that of an axisymmetric nucleus with tude (circulating) and saucer (librating) orbits, described by [21].

We assume that we are in the diffusive (empty) loss cone regime. This assumption has been used in many other theoretical works, and has been confirmed by simulations. The flux can then be estimated as

$$F(E)dE = \frac{N_{lw}(E)dE}{\tau_{relax}} \ . \tag{3.16}$$

We assume an isotropic power law distribution function, i.e. $f(E,\Re,\Re_z) = f(E) = CE^p$. The corresponding mass density is given by $\rho = \rho_0 \left(\frac{r}{r_0}\right)^{-\gamma}$, where $\gamma = p + 3/2$. Here, C is a normalization constant given by $C = 2^{-5/2}\pi^{-1}\left(\frac{GM_1}{r_0}\right)^{-p-3/2}\frac{n_0}{\beta(3/2,p+1)}$ where n_0 is the number density of stars at r_0.

For such a power law distribution, we have

$$M_*(<r) = \frac{4\pi}{3-\gamma}\rho_0 r_0^{\gamma} r^{3-\gamma} \ . \tag{3.17}$$

We define the radius of influence r_h of M_1 as the radius at which the mass enclosed is equal to the BH mass; $M_*(<r_h) = M_1$. An alternative but almost equivalent way is to define it in terms of the flat velocity dispersion σ_0: $r_h = GM_1/\sigma_0^2$.

If we further characterize the density of the cusp by a parameter η such that $r_h = \eta r_0$, we have

$$M_1 = \frac{4\pi}{3-\gamma}\rho_0 r_0^3 \eta^{3-\gamma} \ . \tag{3.18}$$

We can take the three independent parameters of the problem as M_1, r_0, and η, and express ρ_0 and n_0 in terms of these:

$$\rho_0 = \frac{(3-\gamma)M_1}{4\pi r_0^3 \eta^{3-\gamma}} \ , \quad n_0 = \rho_0/m_* \ . \tag{3.19}$$

It is convenient to convert this to a distribution over semimajor axes instead. If we assume that the orbit is nearly Keplerian (with the apsidal precession, GR, and LK effects being perturbations), we have $E = -\frac{GM_1}{2a}$.

$$f(a) = f(E)|\frac{dE}{da}| = C\frac{GM_1}{2a^2}\left(\frac{GM_1}{2a}\right)^p \ . \tag{3.20}$$

We consider the tidal loss cone size l_t to be equal to l_{lc}, as the second term of equation 3.14 is usually negligible compared to the first. The number of stars inside the loss wedge between a and $a+da$ is then given by

$$N_{lw}(a)da = \int\int \mathcal{G}_E f(a,l,l_z)da\,dl\,dl_z = \mathcal{G}_E f(a)da\int_{l_-}^{l_+} dl \int_{-l_t}^{l_t} dl_z \tag{3.21}$$

$$= 2\mathcal{G}_E f(a)\,(l_+ - l_-)\,l_t\,da \tag{3.22}$$

provided that $l_- < l_t$. Here, the integration variables separate out because we are considering spherical symmetry. $\mathcal{G}_E$ is the density of states in spherical (isotropic) geometry:

$$\mathcal{G}_E = \frac{\sqrt{2}\pi^3(GM_1)^3}{E^{5/2}} = 8\pi^3(GM_1)^{1/2}a^{5/2} \ . \tag{3.23}$$

For a SMBHB, the loss cone is never at a completely steady state, because the secondary BH is continuously inspiraling towards the center. In addition, the stellar cusp around the BH can significantly change during the

inspiral, altering the stellar potential. The captures themselves lead to increase of the mass of the BH, which changes the size of the loss cone.

However, if the change to the loss cone size and the stellar cusp is slow enough, they can be treated as adiabatic invariants, and the theory of steady state loss cone dynamics can be applied. The quasi-steady state assumption is assumed here, and is valid to a large degree [23].

The flux of stars into the SMBH, per unit semimajor axis, is then given by equation 2.75 in the limit $q << 1$:

$$F(a) = \frac{N_{lw}(a)}{P_k(a,D)} = \frac{2 \cdot 8\pi^3 (GM_1)^{1/2} a^{5/2} \cdot C \frac{GM_1}{2a^2} \left(\frac{GM_1}{2a}\right)^p \cdot (l_+ - l_-) \cdot l_t}{f_K \frac{\sqrt{M_1}}{\sqrt{GM_2}} \frac{D^3}{a^{3/2}}} \tag{3.24}$$

$$= \frac{2^{-p-1}\pi(3/2-p)}{f_K \beta(3/2, p+1)} G^{1/2} q M_1^{5/3} m_*^{-7/6} r_0^{p-3/2} \eta^{p-3/2} r_*^{1/2} D^{-3} (l_+ - l_-) a^{3/2-p} \tag{3.25}$$

where f_K is the numerical factor of P_k/T_k.

In order to obtain the total flux into the BH, we integrate over the semimajor axis a. We take the upper limit of integration to be $D/2$, as the quadrupolar term in the Hamiltonian scales as $\frac{a^2}{D^3}$. Although the quadrupolar approximation of the Kozai mechanism may not be strictly valid at $a = D/2$, we can use this limit to obtain an upper limit to the flux.

$$\dot{N} = \int_0^{D/2} F(a) da \approx \frac{2^{-p-1}\pi(3/2-p)}{f_K \beta(3/2, p+1)} G^{1/2} q M_1^{5/3} m_*^{-7/6} r_0^{p-3/2} \eta^{p-3/2} r_*^{1/2} D^{-3} \int_0^{D/2} (l_+ - l_-) a^{3/2-p} da \ . \tag{3.26}$$

We can scale the integrand with respect to D:

$$\dot{N}(t) = \int_0^{D/2} F(a) da \approx \frac{2^{-p-1}\pi(3/2-p)}{f_K \beta(3/2, p+1)} G^{1/2} q M_1^{5/3} m_*^{-7/6} r_0^{p-3/2} \eta^{p-3/2} r_*^{1/2} D(t)^{-1/2-p} \int_0^{1/2} (l_+ - l_-) x^{3/2-p} dx \ . \tag{3.27}$$

The above equation, combined with the evolution equations for the binary separation D, give the flux into the loss wedge. Again we emphasize that the above equation is valid only when $l_- < l_+$ among other conditions stated earlier.

This should be combined with the expression for the flux into the loss cone due to two-body relaxation, given by equation 2.66.

$$\dot{N}_S = \int F_S(\mathcal{E}) d\mathcal{E} \ . \tag{3.28}$$

$$\dot{N}_{tot} = \dot{N}_B + \dot{N}_S \ , \tag{3.29}$$

where the subscript S denotes single BH nucleus, and B denotes binary BH nucleus. When the Kozai mechanism is active, $\dot{N}_B >> \dot{N}_S$, so we can concentrate on the former to obtain analytic expressions for the observables.

Since l_+ and l_- are complicated functions of a and D, the integral in equation 3.27 is difficult to perform analytically. However, we can obtain an estimate of the peak capture rate if we assume that, at the appropriate value of $D = D_p$, we have $l_+ \approx 1$ and $l_- \approx 0$ for $0 < a < D/2$. As shown in Appendix A, this is a valid assumption to make:

$$\dot{N}_p = \frac{(3/2-p)2^{-7/2}\pi}{(5/2-p) f_K \beta(3/2, p+1)} G^{1/2} q M_1^{5/3} m_*^{-7/6} r_0^{p-3/2} \eta^{p-3/2} r_*^{1/2} D_p^{-1/2-p} \ , \tag{3.30}$$

$$= \frac{(3-\gamma)2^{-7/2}\pi}{(4-\gamma) f_K \beta(3/2, \gamma-1/2)} G^{1/2} q M_1^{5/3} m_*^{-7/6} (\eta r_0)^{\gamma-3} r_*^{1/2} D_p^{1-\gamma} \tag{3.31}$$

(subscript p denotes peak).

When does this peak occur? We expect that the Kozai mechanism is at its strongest when the two competing mechanisms, SP precession and GR precession, cancel out each other. This is possible only because the precession

due to these effects are in opposite directions.

$$\left(\frac{d\omega}{dt}\right)_{SP} + \left(\frac{d\omega}{dt}\right)_{GR} = 0 \implies \frac{3(GM_1)^{3/2}}{a_p^{5/2}c^2(1-e^2)} = \sqrt{\frac{GM_1}{a_p^3}}\sqrt{1-e^2}\left(\frac{M_*}{M_1}\right) \tag{3.32}$$

$$a_p = \frac{3GM_1^2}{l^{3/2}c^2M_*} \ . \tag{3.33}$$

Substituting for $M_*(a) = 4\pi\rho_0 r_0^\gamma \frac{a^{3-\gamma}}{3-\gamma}$, we have

$$\begin{aligned} a_p^{4-\gamma} &= \frac{3GM_1^2(3-\gamma)}{l^{3/2}c^2 \times 4\pi\rho_0 r_0^\gamma} \ , \\ &= \frac{3GM_1}{l^{3/2}c^2}(r_0^{3-\gamma}\eta^{3-\gamma}) \ . \end{aligned}$$

We can assume a value of $l = l_T$ for the purpose of getting an estimate of a_p:

$$a_p = \left(\frac{3GM_1^{3/4}}{2^{3/4}c^2} r_0^{3-\gamma}\eta^{3-\gamma}\frac{m_*^{1/4}}{r_*^{3/4}}\right)^{1/(\frac{13}{4}-\gamma)} \tag{3.34}$$

and $D_p = 2a_p$.
Thus, the final expression for the peak capture rate during the enhanced phase is

$$\dot{N}_p = C_\gamma \times c^{\frac{-8(1-\gamma)}{13-4\gamma}} \times G^{\frac{1}{2}+\frac{4(1-\gamma)}{13-4\gamma}} \times q \times M_1^{\frac{5}{3}+\frac{3(1-\gamma)}{13-4\gamma}} \times (\eta r_0)^{(\gamma-3)+\frac{4(3-\gamma)(1-\gamma)}{13-4\gamma}} \times m_*^{-\frac{7}{6}+\frac{1-\gamma}{13-4\gamma}} \times r_*^{\frac{1}{2}-\frac{3(1-\gamma)}{13-4\gamma}} \ , \tag{3.35}$$

where,

$$C_\gamma = \left[\frac{(3-\gamma)2^{-7/2}\pi}{(4-\gamma)f_K\beta(3/2,\gamma-1/2)} \times 2^{1-\gamma}\left(\frac{3}{2^{3/4}}\right)^{\frac{4(1-\gamma)}{13-4\gamma}}\right] \ . \tag{3.36}$$

We can use these expressions to obtain an approximate result for the capture rate vs time. Dividing equation 3.27 by 3.30,

$$\frac{\dot{N}(t)}{\dot{N}_p} = 2^{5/2-p}\,(5/2-p)\left(\frac{D}{D_p}\right)^{-1/2-p}\int_0^{1/2}(l_+ - l_-)x^{3/2-p}dx \ . \tag{3.37}$$

The value of the integral was analyzed as a function of D and the input parameters. The best fit curve is

$$\int_0^{1/2}(l_+ - l_-)x^{3/2-p}dx = \begin{cases} \frac{cd^{1.5}}{5.36+d^3} + k & D_{min} \le D \le D_{max} \\ 0 & \text{otherwise} \end{cases} \tag{3.38}$$

where $d = D/D_p$, and c and k is a function of the input parameters, of the order $c \sim 10^{-1}$ and $k \sim 10^{-2}$.D_{min} and D_{max} are described in the next section. More details are in Appendix A.
Therefore, the capture rate during the enhanced phase ($D_{min} \le D \le D_{max}$) is approximated by

$$\frac{\dot{N}(t)}{\dot{N}_p} = 2^{5/2-p}\,(5/2-p)\,d^{-1/2-p}\left(\frac{cd^{1.5}}{5.36+d^3} + k\right) \ . \tag{3.39}$$

3.3 Duration of Enhanced Phase

As mentioned, the conditions for enhancement of capture rate for a SMBHB system are $l_{fp} \le 1$, $l_- < l_+$, and $l_- \le l_t$. It is difficult to analytically derive the values of a and D when all three conditions are satisfied. However, we can obtain some approximate conditions by considering the cases were $D, a \gtrsim 1$ pc, where GR effects are negligible, and $D, a \lesssim 0.1$ pc, where stellar precession is negligible.
The changes in angular momentum due to the Kozai mechanism take place on a timescale $t_k = \left(\frac{1}{L}\frac{dL}{dt}\right)^{-1}$. The specific angular momentum is given by $L = \sqrt{GM_1 a(1-e^2)}$, and the torque due to the quadrupolar force of the

secondary BH is

$$\frac{dL}{dt} = |r \times F| \sim \frac{qGM_1a^2}{D^3} \ . \tag{3.40}$$

Thus, the instantaneous Kozai timescale is given by

$$t_K = \frac{D^3}{q\sqrt{GM_1a^3}}\sqrt{1-e^2} = T_K\sqrt{1-e^2} \ , \tag{3.41}$$

which is just $\sqrt{1-e^2} = l$ times the Kozai timescale. The l factor shows that when the angular momentum is low, the instantaneous timescale t_K is much smaller than the overall timescale T_K, as the torques required to change the angular momentum is also low.

We first examine the stellar precession dominated region. The timescale for SP precession is given by $T_{SP} = |\frac{1}{\pi}\left(\frac{d\omega}{dt}\right)_{sp}|^{-1}$. If the Kozai mechanism is to operate, the Kozai precession timescale must be lesser than the timescale for SP precession.

Thus we have

$$\frac{\pi M_1}{\sqrt{1-e^2}}\frac{3-\gamma}{4\pi\rho_o a^3}\left(\frac{a}{r_0}\right)^\gamma\sqrt{\frac{a^3}{GM_1}}\frac{1}{G_M(e,\gamma)} > \sqrt{1-e^2}\frac{\sqrt{M_1}}{\sqrt{G}M_2}\frac{D^3}{a^{3/2}} \ . \tag{3.42}$$

The value of the numerical factor $G_M(e,\gamma)$ for highly eccentric orbits is close to 1, so we disregard this factor. As explained earlier, the largest value of a that we consider in the quadrupolar approximation is $D/2$. Putting this limit in, we have

$$D < \left(\frac{(3-\gamma)M_2}{2^{\gamma+2}\rho_0 r_0^\gamma l^2}\right)^{1/(3-\gamma)} \ . \tag{3.43}$$

For capture rate enhancement to occur, the value of l must be substantially different from l_t. A reasonable value is to take $l = 0.1$, which is much larger than the "typical" value of $l_t \sim 0.01$.

Thus, D_{max} has a scaling of $\propto \left(\frac{qM_1}{\rho_0 r_0^\gamma}\right)^{1/(3-\gamma)}$. Substituting for ρ_0,

$$D_{max} = \left(\frac{\pi}{2^\gamma}\right)^{1/(3-\gamma)}\left(\frac{q}{0.01}\right)^{1/(3-\gamma)}\left(\frac{r_0\eta}{1\text{ pc}}\right) \quad \text{pc} \ . \tag{3.44}$$

On the other hand, when the binary separation is in the sub-parsec scales, GR will be the dominating mechanism. The minimum value of D of the enchanced phase can be estimated by considering again the cancellation between SP and GR effects:

$$a_{min} = \left(\frac{3GM_1}{l^{3/2}c^2}(r_0\eta)^{3-\gamma}\right)^{1/(4-\gamma)} \ . \tag{3.45}$$

For capture rate enhancement to occur, we argue that $l > 0.1$ as before. Putting in $D_{min} = 2a_{min}$, we have

$$D_{min} = 2\left(\frac{3GM_1(r_0\eta)^{3-\gamma}}{c^2(0.1)^{3/2}}\right)^{1/(4-\gamma)} \tag{3.46}$$

Therefore, the duration of the enhanced capture rate is $T_e = t(D_{max}) - t(D_{min})$, which mainly corresponds to phase 2 of the SMBHB evolution. Because the binary evolution is not governed by a single equation, it is necessary to add the time spent in each of the phases of section 2.3 between D_{max} and D_{min}.

In phase 1, the secondary inspirals due to dynamical friction. We can use equation 2.78 to obtain an expression for the binary separation D as a function of time:

$$D_0^{3-\gamma/2} - D^{3-\gamma/2} = \sqrt{\frac{G}{M_1}}M_2\ln\Lambda(\eta r_0)^{\frac{3-\gamma}{2}}(3-\gamma/2)F(\gamma)\ t \ , \tag{3.47}$$

where D_0 is the initial separation. Note that the evolution equation is slightly changed because we take $r_h = \eta r_0$, unlike in equation 2.78 where $r_h = r_0$.

We want the time spend by the secondary in phase 1 during the TDE enhancement phase, which corresponds to

evolution from D_{max} to r_h:

$$t_1 = \frac{max(D_{max}, r_h)^{3-\gamma/2} - r_h^{3-\gamma/2}}{\sqrt{\frac{G}{M_1}} M_2 \ln\Lambda (\eta r_0)^{\frac{3-\gamma}{2}} F(\gamma)(3-\gamma/2)} \ . \tag{3.48}$$

Obviously, if $D_{max} \leq r_h$ we have $t_1 = 0$.

The next stage of the binary evolution (stage 2) corresponds to the hardening of the binary. The inspiral is governed by equation 2.82:

$$\frac{dr}{dt} = -\mathcal{H}\frac{G\rho r^2}{\sigma} dt \ . \tag{3.49}$$

In this phase, $\mathcal{H}$ can be approximated as $\mathcal{H} \approx q\mathcal{H}_\infty \approx 16q$ [21].

Substituting for $\rho = \rho_0 \left(\frac{r}{r_0}\right)^{-\gamma}$ and $\sigma = \sigma_0\sqrt{1+\frac{r_h}{r}}$, we have

$$dr \ r^{\gamma-5/2}\sqrt{r+r_h} = -\frac{\mathcal{H}G\rho_0 r_0^\gamma}{\sigma_0} dt \ . \tag{3.50}$$

We wish to integrate this expression from $r_1 = min(r_h, D_{max})$ to $r_2 = max(a_h, D_{min})$. Change of variables from r to $x = r/r_h$ gives

$$r_h^{\gamma-1} \int_{x_1}^{x_2} dx \ x^{\gamma-5/2}\sqrt{x+1} = \frac{\mathcal{H}G\rho_0 r_0^\gamma}{\sigma_0} t_2 \ . \tag{3.51}$$

Calling the value of the above integral as I, we have

$$t_2 = \frac{I\sigma_0 \eta^{\gamma-1}}{\mathcal{H}G\rho_0 r_0} \ . \tag{3.52}$$

The final phase of binary evolution is the hardening due to collisional loss cone repopulation. Equation 2.88 can be used to express the time taken for the separation to shrink from a_h to D_{min}. During the enhanced phase, our theory and other N-body simulations tell us that the binary spends very little, if any, time in phase 3. Thus, it is a reasonable approximation to take the coefficient $\mathcal{D} = \mathcal{D}_0$, its value at a_h:

$$t_3 = \frac{1}{\mathcal{D}_0}\left(\frac{a_h^2}{min(a_h^2, D_{min}^2)} - 1\right) \ . \tag{3.53}$$

Thus, the duration of enhanced capture rate is

$$t_e = t_1 + t_2 + t_3 \ . \tag{3.54}$$

We note that for most of our parameter choices, $t_2 >> t_1, t_3$, implying that the enhanced phase roughly corresponds with phase 2 of the SMBHB evolution paradigm.

Chapter 4

Results

4.1 Parameter Space

Throughout the work, we have assumed a power law density $\rho = \rho_0 \left(\frac{r}{r_0}\right)^{-\gamma}$, with r_0 being associated with the radius of influence of the BH r_h as $r_h = \eta r_0$. We recall that the radius of influence is defined as $M(< r_h) = M_1$. The value of ρ_0 is therefore determined by the parameters M_1, r_0, and γ.

This density profile corresponds to an isotropic distribution function $f(E) = CE^p$ with $p = \gamma - 3/2$. The isothermal model $\rho \propto r^{-2}$ is a well-established model; however this is applicable only in the outer parts of galaxies, well beyond the radius of influence. Adiabatic growth of the SMBH (Bahcall-Wolf cusp) corresponds to a density profile $f(E) \propto E^{1/4}$ at very close distances, which implies a value of $\gamma = 7/4$ [1].The lower limit of γ is $1/2$, as $p = -1$ is the shallowest density profile that is consistent with an isotropic distribution function [21]. We consider values of γ in the range from 0.7 to 1.75.

The mass of supermassive black holes in galactic nuclei vary across many orders of magnitudes, from $10^6 M_\odot$ to $10^9 M_\odot$. The mass of Sagittarius A*, the supermassive black hole at the center of the Milky Way, has a mass $4 \times 10^6 M_\odot$. However, there are several constraints on M_1 and q in our model. Firstly, as explained before, a star's capture is observed as a tidal disruption event only if the tidal radius is greater than the Schwarzschild radius. This induces an upper limit of M_1 as $10^8 M_\odot$ for solar mass solar radius stars. Secondly, since M_2 is itself a supermassive black hole, qM_1 must be in the SMBH mass range. The Lidov-Kozai effect is applicable only to hierarchical three-body systems, so the value of q should be in the range range $0.01 - 0.1$. Therefore we consider M_1 in the range $10^7 - 10^8 M_\odot$.
Finally, the ranges of r_0 and η are to be determined. We saw in the previous section that all the observables depend only on the combination $r_h = \eta r_0$. The radius of influence of Sagittarius A* is around 3 pc. We consider values of ηr_0 were taken to be from $0.5 - 5$ pc.
In table 4.1, we list some key parameter choices which are of interest to us, which help determine the overall trend of the observables.

In addition to these, there are other parameters which indirectly come into account. The stellar velocity dispersion, in the isotropic case, can be estimated as

$$\sigma^2 = \frac{GM}{r}\left(1 + \frac{r}{r_h}\right) = \sigma_0^2\left(1 + \frac{r_h}{r}\right) \ , \tag{4.1}$$

that is, a dispersion profile with a $r^{-1/2}$ dependence near the center and flattens out to a constant at large distances. A flat rotation curve has been observed at the edges of most galaxies. The value of σ_0 is given by the famous M-σ relation [8]:

$$\left(\frac{M_1}{10^8 M_\odot}\right) = (1.66 \pm 0.32)\left(\frac{\sigma_0}{200 km/s}\right)^{4.58 \pm 0.52} \ . \tag{4.2}$$

Table 4.1: Parameter space

Model No.	$\mathbf{M_1}$	q	γ	$\eta\mathbf{r_0}$
1	$10^7 M_\odot$	0.01	1.75	1 pc
2	$10^7 M_\odot$	0.01	1.5	1 pc
3	$10^7 M_\odot$	0.01	1.2	1 pc
4	$10^7 M_\odot$	0.01	1	1 pc
5	$10^7 M_\odot$	0.01	0.7	1 pc
6	$10^7 M_\odot$	0.02	1.5	1 pc
7	$10^7 M_\odot$	0.03	1.5	1 pc
8	$10^7 M_\odot$	0.05	1.5	1 pc
9	$2 \times 10^7 M_\odot$	0.01	1.5	1 pc
10	$3 \times 10^7 M_\odot$	0.01	1.5	1 pc
11	$5 \times 10^7 M_\odot$	0.01	1.5	1 pc
12	$10^8 M_\odot$	0.01	1.5	1 pc
13	$10^7 M_\odot$	0.01	1.5	0.5 pc
14	$10^7 M_\odot$	0.01	1.5	2 pc
15	$10^7 M_\odot$	0.01	1.5	3 pc
16	$10^7 M_\odot$	0.01	1.5	5 pc

The value of σ is important in the evolution of the SMBHB, especially in phase 2. As the enhancement in capture rates occurs primarily in phase 2, the velocity dispersion profile affects the duration of the phase of enhancement. In our model, we have considered the galaxy to be composed entirely of solar mass solar radius stars. In a real galaxy, there is a distribution of stellar masses and radii. This can be taken into account by including additional terms to the distribution function

$$f(\mathcal{E}) \rightarrow f(\mathcal{E}, m, r) = f(\mathcal{E})\xi_m(m)\xi_r(r) \tag{4.3}$$

where ξ_m and ξ_r are the stellar mass and radius profiles respectively. The corresponding tidal radius and the size of the loss cone will be a function of ξ_m and ξ_r, which can alter the TDE rates.

4.2 Results

The capture rate and the binary separation as a function of time for model 2 (q=0.01, $M_1 = 10^7 M_\odot$, $\gamma = 1.5$, $\eta r_0 = 1$ pc are shown in figures 4.1 and 4.2.

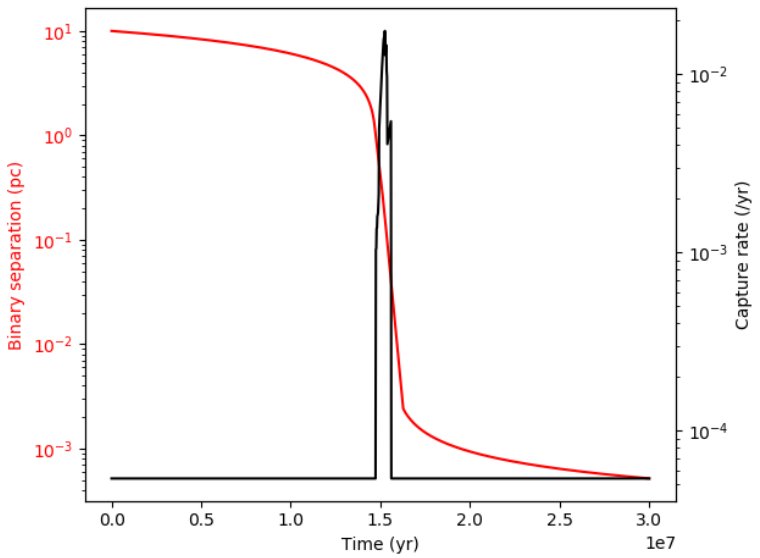

Figure 4.1: Left: binary separation in pc. Right: capture rate (/yr)

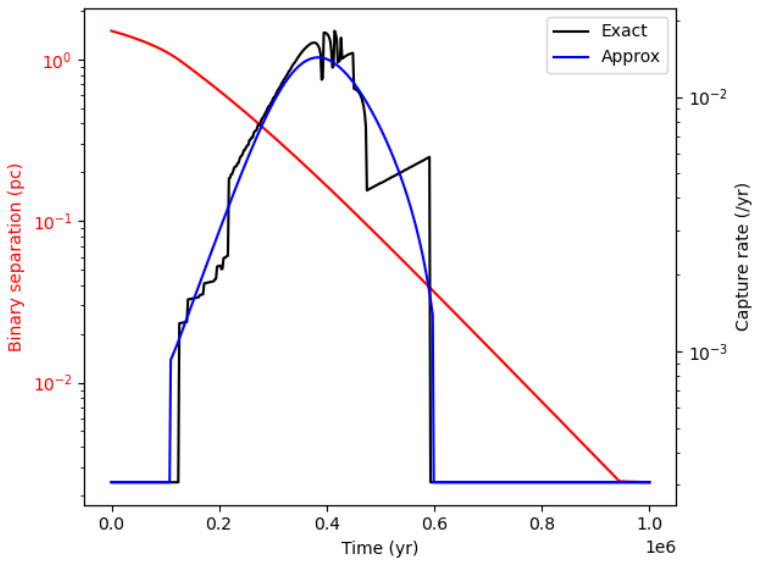

Figure 4.2: Figure 4.1 zoomed in, along with the approximation equation 3.39

The sudden and sharp rise and fall of the capture rate are due to our condition that a capture occurs only if $l_{min} \leq l_{lc}$. In reality, if $l_{min} \gtrsim l_{lc}$, the star can undergo complex chaotic three-body interaction with the binary system which may or may not result in a TDE.

We calculate the peak capture rate, the starting and stopping separations of the enhanced phase, and the duration of enhancement for each of the models in table 4.1. We tabulate the results from the full model, the results from the equations 3.30, 3.44, 3.46, and 3.54, and the percentage errors between the two.

The approximation formulas listed above provide a reasonable estimate of the observables $\dot{N}_p$ and T_e, with an error of about 20% for both. The approximations get worse as the mass ratio q increases.

From the table, we see that the general trend of the calculations is as follows:

- The enhanced capture rate phase begins when the binary separation reaches $\sim r_h$.
- The enhanced phase ends when the binary separation reaches $\sim a_h$.
- The duration of the enhanced phase is generally of the order of $\sim 10^5 - 10^6$ yr, with the last model reaching $\sim 10^7$ yr. The duration is a strong function of ηr_0.
- As the mass ratio q increases, the value of D_{max} increases and D_{min} decreases. This is because the Kozai effect is more powerful, and can remain effective for a larger range of D. However, with increasing q, M_2 inspirals towards M_1 faster, so the duration of the enhanced phase is of the same order of magnitude.
- The peak capture rate $\dot{N}_p$ is 2-3 orders of magnitude higher than the typical capture rate of nuclei containing a single SMBH. It is a strong function of all the four parameters.

Table 4.2: Results of the full model and analytic approximations for the various parameter choices listed in table 4.1

Model	Full Model					Approximation					Error %				
	$\dot{N}_p$ (/yr)	D_p (pc)	D_{max} (pc)	D_{min} (pc)	T_e (Myr)	$\dot{N}_p$ (/yr)	D_p (pc)	D_{max} (pc)	D_{min} (pc)	T_e (Myr)	$\dot{N}_p$	D_p	D_{max}	D_{min}	T_e
1	0.045	0.1034	0.8686	0.0251	0.3876	0.0499	0.0822	0.9468	0.0238	0.4081	9.62	20.51	9.01	5.09	5.28
2	0.0176	0.1694	0.9955	0.0394	0.4602	0.0172	0.1297	1.0725	0.0371	0.4826	2.19	23.44	7.74	5.8	4.87
3	0.0069	0.2392	1.1141	0.0575	0.5598	0.0059	0.1936	1.1899	0.0569	0.5833	15.1	19.09	6.8	1.04	4.2
4	0.0037	0.2851	1.1844	0.0722	0.632	0.0029	0.2382	1.2533	0.0721	0.6571	21.01	16.45	5.82	0.16	3.97
5	0.0011	0.4358	1.2638	0.0853	0.8262	0.0008	0.306	1.3321	0.0975	0.788	31.06	29.79	5.41	14.31	4.63
6	0.0434	0.1658	1.5757	0.0209	0.3452	0.0344	0.1297	1.7025	0.0371	0.3304	20.67	21.75	8.05	77.92	4.3
7	0.0765	0.1668	2.0663	0.0109	0.322	0.0516	0.1297	2.2309	0.0371	0.2972	32.54	22.23	7.97	238.94	7.72
8	0.1662	0.2095	2.9048	0.005	0.2598	0.086	0.1297	3.1361	0.0371	0.2949	48.26	38.1	7.96	648.05	13.51*
9	0.0459	0.1821	1.0035	0.0627	0.2318	0.0471	0.1746	1.0725	0.049	0.2596	2.56	4.13	6.88	21.9	12
10	0.0795	0.213	1.0087	0.0815	0.1544	0.0848	0.2077	1.0725	0.0576	0.1803	6.74	2.49	6.32	29.37	16.79
11	0.155	0.286	1.0201	0.1063	0.0941	0.1781	0.2585	1.0725	0.0706	0.1137	14.89	9.61	5.13	33.59	20.83
12	0.3849	0.2849	1.0492	0.1505	0.0489	0.4875	0.348	1.0725	0.0932	0.0606	26.64	22.12	2.22	38.07	23.87
13	0.0609	0.091	0.4985	0.0254	0.1071	0.0655	0.0716	0.5363	0.0245	0.1132	7.55	21.36	7.56	3.54	5.72
14	0.0054	0.2588	1.9833	0.0556	2.0153	0.0045	0.235	2.145	0.0562	2.0554	16.98	9.2	8.16	1.17	1.99
15	0.0027	0.327	2.9819	0.0662	4.8018	0.0021	0.3326	3.2175	0.0717	4.7939	23.59	1.72	7.9	8.35	0.16
16	0.0011	0.4377	4.02	0.0863	13.1989	0.0008	0.5153	5.3626	0.0974	13.9191	31.11	17.72	33.4	12.86	5.46

*Since the values of D_{min} from the approximation and the full model differ greatly, we use the same value of D_{min} to calculate T_e in both cases.

4.3 Scaling Relations

In figure 4.3, we have a log-log plot of $\dot{N}_p$ as a function of M_1 for different values of γ. The other parameters, q and ηr_0, are set as 0.01 and 1 pc respectively. The linear relation in the log-log plot shows the validity of the approximation $\dot{N}_p \propto M_1^{\frac{5}{3}+\frac{3(1-\gamma)}{13-4\gamma}}$.

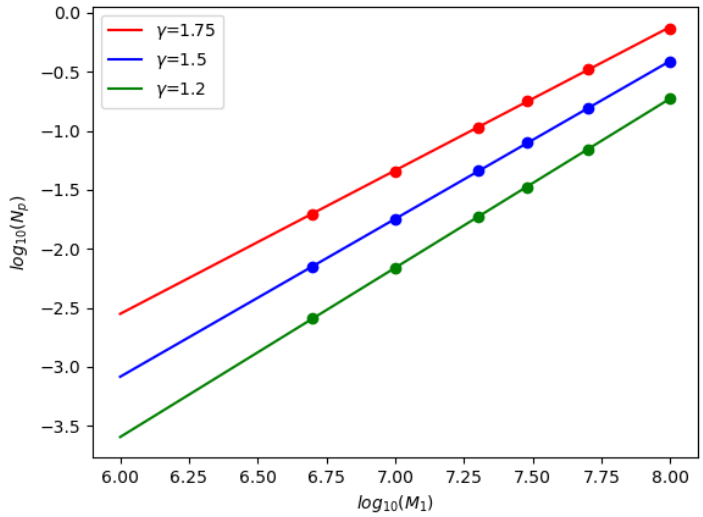

Figure 4.3: $log(\dot{N}_p)$ as a function of $log(M_1)$

Table 4.3: Slopes of $\log(\dot{N}_p)$ vs $\log(M_1)$

γ	**Best fit slope**	$\frac{5}{3}+\frac{3(1-\gamma)}{13-4\gamma}$
1.75	1.216	1.292
1.5	1.338	1.452
1.2	1.434	1.593

Next, we examine the relation between $\dot{N}_p$ and γ. Equation 3.30 give us that a plot of $log(\dot{N}_p)$ vs γ should be a straight line. Figure 4.4 confirms the validity of this result. The other parameters are set to $M_1 = 10^7 M_\odot$, $q = 0.01$, and $\eta r_0 = 1$ pc.

In figure 4.5, $\dot{N}_p$ is plotted against q for different values of M_1. Our model and our data predict a linear relationship between the two, with $\gamma = 1.5$ and $\eta r_0 = 1$ pc. It is noted that our model is limited by the range of M_1 and q that we can explore.

Finally, figure 4.6 shows $\dot{N}_p$ as a function of $r_h = \eta r_0$. A plot of $log(\dot{N}_p)$ vs $log(r_h)$ should be a straight like with slope $(\gamma - 3) + \frac{4(3-\gamma)(1-\gamma)}{13-4\gamma}$ from equation 3.30, and this is confirmed in figure 4.6. Solid line is for $M_1 = 10^7 M_\odot$, and dashed line is for $M_1 = 3 \times 10^7 M_\odot$.

Table 4.4: Slopes of $\log(\dot{N}_p)$ vs $\log(r_h)$

γ	**Slope for** $M_1 = 10^7 M_\odot$	**Slope for** $M_1 = 3 \times 10^7 M_\odot$	$(\gamma - 3) + \frac{4(3-\gamma)(1-\gamma)}{13-4\gamma}$
1.75	-1.634	-1.653	-1.875
1.5	-1.730	-1.755	-1.928
1.2	-1.813	-1.821	-1.976

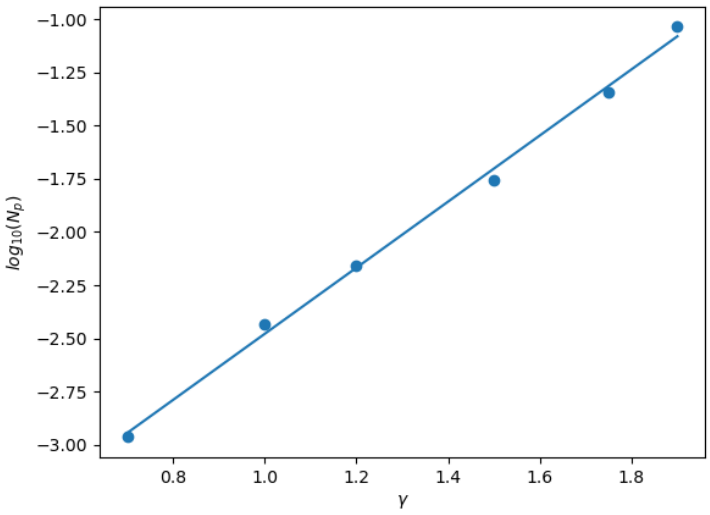

Figure 4.4: $\log(\dot{N}_p)$ as a function of γ

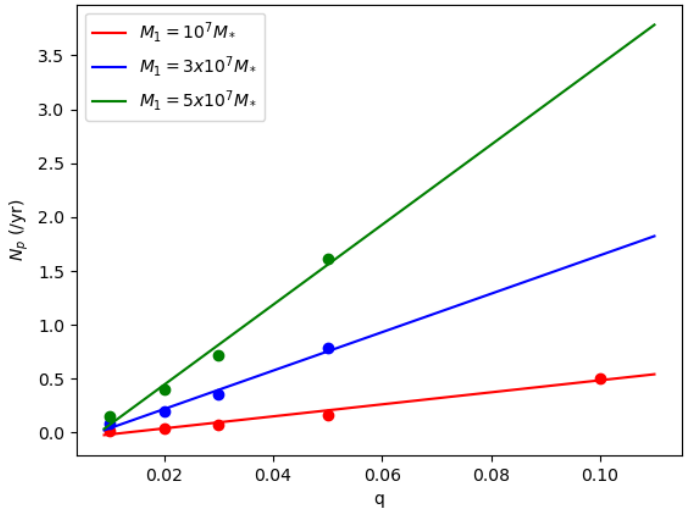

Figure 4.5: $\dot{N}_p$ as a function of q

4.4 Comparison with Earlier Studies

Ivanov et. al. [13] were among the first to explore the tidal disruption rate enhancement due to the presence of a secondary black hole. They considered only the Kozai effect and the stellar apsidal precession, and they considered only dynamical friction as the only mechanism of inspiral of the secondary BH. Their results showed that for a dense cusp of size ~ 1 pc and $q \sim 0.01$, the TDE rate during the enhanced phase can reach $10^{-2} - 1 M_\odot$ yr^{-1}. The duration of this enhancement was found to be 6×10^4yr. This is comparable to our model number 2, where the peak rate is 0.018 $M_\odot$ yr^{-1} and the duration of enhancement is 4.6×10^5yr. The rate from our model is lower than theirs because we have considered the effect of GR precession which can destroy the Kozai effect, significantly decreasing the TDE rate. In addition, the duration of the enhanced phase in our model is higher because we consider the evolution of the binary to be dominated by hardening and secondary slingshot mechanisms at $D \leq r_h$. For a value of $\gamma = 3/2$, they obtained a scaling relation of $\dot{N}_p \propto q^{4/3} M_1^{5/3} r_0^{-2}$. This can be compared to our expression of $\dot{N}_p \propto q M_1^{1.45} r_h^{-1.93}$ for $\gamma = 3/2$, which show similar scaling relations.

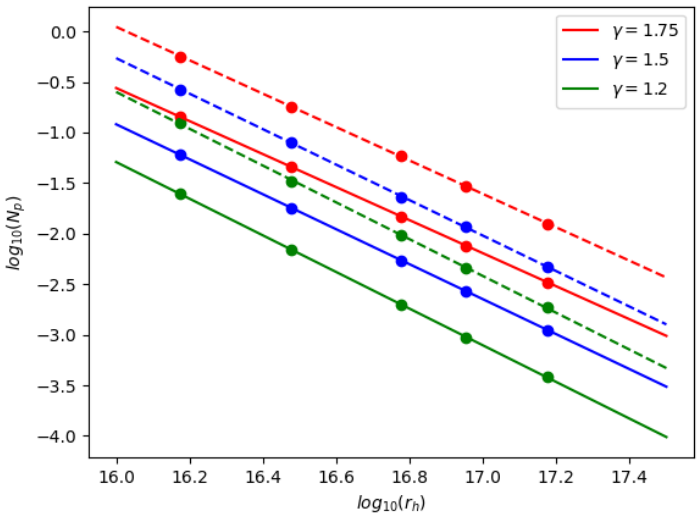

Figure 4.6: $\log(\dot{N}_p)$ as a function of $\log(r_h)$

Using numerical scattering experiments, Chen et. al. [6] [7] investigated the TDE rates of binaries entering the hardening stage, i.e. late half of phase 2. They obtained a scaling relation as $\dot{N}_p \propto q^{(4-2\gamma)/(3-\gamma)} \left(\frac{D}{a_h}\right) M_1^{-1/3}\sigma^4$. For a mass $M_1 = 10^7 M_\odot$ and $q = 1/81$ embedded in an isothermal cusp, they obtained a peak value of $\dot{N}_p \approx 0.2$ yr^{-1} for a duration of $\approx 3 \times 10^5$ yr. This is comparable to our result of $\dot{N}_p \approx 0.1$ yr^{-1} for a duration of 3.4×10^5 yr when a value of $\gamma = 1.9$ ($\gamma = 2$ causes divergences in our model). A value of $\gamma = 1.5$ in their model gives the peak TDE rate as $\approx 10^{-2}$ yr^{-1}. However, in their model most of the stars which ended up tidally disrupted were on chaotic orbits due to three-body interactions with the binary. Naturally, it is expected that their model would yield different scaling relations and results. It is worth noting that their results, obtained from direct numerical simulations, are in good agreement with ours, which are obtained from theoretical stellar dynamics.

Similar results were obtained by a study by Lui and Chen [17], who obtained a rate of $\sim 10^{-2}$ yr^{-1} for the same parameters. Wegg and Bode [3] studied EMRIs in nuclei containing a binary black hole, and found an enhancement of about two orders of magnitude. Lezhnin and Vasiliev [15] explored the TDE rates in systems of various geometries containing a SMBHB. For spherical systems, they found an increase by two to three orders of magnitude, for a time period of $\sim 10^7$ yr for $M_1 = 10^7 M_\odot$. However, they did not derive any explicit scaling relations.

Recent studies by Li et. al. [4] [5] explored the tidal disruption rates during equal and unequal mass galaxy mergers by using direction N-body simulations. They found that for the case of equal mass mergers, the TDE enhancement is only boosted by a few times. However for unequal mass mergers ($q \sim 0.1 - 0.5$), the rates can be enhanced by an order of magnitude compared to isolated galaxies. Similar to our model, their binary evolution is divided into three phases. They derived a scaling relation as $\dot{N} \propto M_1^{3/2} r_{1/2}^{-2.23} r_t^{0.73}$ for the phase 2 of the binary evolution, where $r_{1/2}$ is the galaxy half-mass radius and r_t is the tidal radius. Their model is limited to sufficiently high mass ratios and do not consider the effectiveness of the Kozai mechanism in their analytic model. Therefore, a direct comparison between their model and ours is not applicable.

In summary, the results of our model match reasonably well with the models of [13] and [7], and the scaling relations we have developed are similar to the scaling relations of their models. A complete extrapolation from our model to other direct numerical simulations require analysis of chaotic orbits that interact strongly with the binary system. However, the effectiveness of the Kozai mechanism, and its suppression by GR and stellar

potential effects, is evident from our analytical model, and match well with existing results.

Chapter 5

Conclusion

In this project, we have examined the tidal disruption rates in galactic nuclei containing a supermassive binary black hole with unequal masses. Such a setup is representative of the late stages of a minor merger. To simplify the setup, we have assumed that the primary BH is stationary at the center, the secondary BH is in an almost circular orbit which spirals toward the primary, and the field stars are distributed according to a power law distribution centered at the primary BH. The field stars move under the influence of the primary and secondary BHs, gravitational effects of the cusp, and general relativity. The stellar dynamics of the field stars is very interesting, with our primary investigation being the angular momentum oscillations due to the Lidov-Kozai effect, stellar precession, and general relativity. Throughout most of the evolution of the binary, the LK effect is completely suppressed by the two competing mechanisms. However, there is a short window of time when the stellar precession and GR precession cancel each other, allowing the LK effect to dominate.

The flux of stars into the loss cone is obtained by solving the axisymmetric Fokker-Planck equation. We have developed analytic results for the peak capture rate and the duration of enhancement. These expressions are a function of M_1, M_2, r_h, γ, and the properties of the field stars. An expression for the TDE as a function of binary separation (which in turn is a function of time) is obtained by semi-analytic means. Our general results show that the TDE rate is increases by two to three orders of magnitude compared to TDE rates of isolated black holes, and the duration of this enhanced phase is $10^5 - 10^6$ years. These results are in agreement with previous works on this topic, such as [13] and [6].

Enhanced TDE rates in galactic nuclei can be used as a method to identify minor mergers. Multiple TDEs originating in a nucleus that are observed during a survey, like the LSST, indicate the possibility of the presence of a binary black hole [26, 30].

Our model explores a limited range of parameters for the mass of the black holes, as the Lidov-Kozai mechanism is present in hierarchical three-body systems. In addition, tidal disruption events are observable only if the tidal radius is greater than the Schwarzschild radius, which sets an upper limit of M_1 as $\approx 10^8 M_\odot$. Further work include exploring a full range of parameters. Specifically, the TDE rates during major mergers, where the black holes are of comparable mass, is to be explored from an analytic point of view. In addition, the flux of stars into the loss cone of the secondary BH, which can further increase the overall TDE rate, is to be addressed. From an observational point of view, an integral over the cosmic volume is to be performed, in order to calculate the number of TDEs which will be observable from Earth, and the fraction of the TDEs which originate in SMBHBs. The probability of a multiple-TDE galaxy hosting a SMBHB is to be calculated. Our novel analytical model may provide more accurate predictions for the observable TDE rates and lead to new exploration in the field of galaxy mergers.

References

[1] J.N. Bahcall and R.A. Wolf. *ApJ*, 209:214:232, 1976. 25

[2] J. Binney and S. Tremaine. *Galactic Dynamics*. Princeton University Press, Princeton, 2008. 13

[3] N. Bode and C. Wegg. *MNRAS*, 438:573:589, 2013. 18, 31, 36

[4] S. Li et al. *ApJ*, 834:195, 2017. 2, 31

[5] S. Li et al. *ApJ*, 883:132, 2019. 2, 31

[6] X. Chen et al. *ApJ*, 697:L149:L152, 2009. 31, 33

[7] X. Chen et al. *ApJ*, 729:13:28, 2011. 2, 31

[8] L. Ferrarese. *ApJ*, 578:90:97, 2002. 25

[9] J. Frank and M.J. Rees. *MNRAS*, 176:633–647, 1976. 10

[10] J. Frank and M.J. Rees. *MNRAS*, 176:633:647, 1976. 1

[11] H. Goldstein, C. Poole, and J. Safko. *Classical Mechanics, 3rd Edition*. Addison-Wesley, Boston, 2001. v, 5, 7

[12] J.G. Hills. *Nature*, 254:295, 1975. 1

[13] P.B. Ivanov, A.G. Polnarev, and P. Saha. *MNRAS*, 358:1361–1378, 2005. 2, 9, 18, 30, 31, 33, 36

[14] Y. Kozai. *AJ*, 67:591, 1962. 8

[15] K. Lezhnin and E. Vasiliev. *MNRAS*, 484:2851:2865, 2019. 31

[16] M.L. Lidov. *Planetary Space Sci.*, 9:719:759, 1962. 8

[17] F.K. Liu and X. Chen. *ApJ*, 767:18, 2013. 2, 31

[18] T. Mageshwaran and A. Mangalam. *ApJ*, 814:141:161, 2015. 1, 12

[19] J. Magorrain and S. Tremaine. *MNRAS*, 309:447–460, 1999. 1, 10, 13

[20] D. Merritt. *ApJ*, 648:976–986, 2006. 13

[21] D Merritt. *Dynamics and Evolution of Galactic Nuclei*. Princeton University Press, Princeton, 2013. 8, 9, 10, 11, 12, 13, 14, 18, 20, 24, 25

[22] M. Milosavljevic and D. Merritt. *ApJ*, 563:34–62, 2001. 1, 13

[23] M. Milosavljevic and D. Merritt. *ApJ*, 596:860–878, 2003. 15, 21

[24] G.D. Quinlan. *New Astronomy*, 1:35:56, 1996. 1

[25] M.J. Rees. *Nature*, 333:523:528, 1988. 1

[26] S. Thorp, E. Chadwick, and A. Sesana. *MNRAS*, 488:4042:4060, 2019. 33

[27] M. Valtonen and H. Karttunen. *The Three-Body Problem*. Cambridge University Press, New York, 2006. 6, 7, 8

[28] E. Vasiliev and D. Merritt. *ApJ*, 774:87–112, 2013. 13

[29] J. Wang and D. Merritt. *ApJ*, 600:149:161, 2004. 1

[30] C. Wegg and N. Bode. *ApJ*, 738:L8, 2011. 33

Appendix A

Angular Momentum Oscillation

Here, we study the behavior of l_+ and l_-, and more importantly $l_+ - l_-$, in order to better understand the capture rate as a function of time.

We recall that under the effects of the LK mechanism, general relativity, and the stellar potential, a field star's angular momentum oscillates between l_+ and l_-, which are the solutions to

$$\Lambda^2 = \frac{3+k}{5}(1-e_+^2)(1-e_-^2) - \frac{B}{5}\left(\frac{\left(\sqrt{1-e_-^2}-\sqrt{1-e_+^2}\right)\sqrt{(1-e_+^2)(1-e_-^2)}}{e_+^2-e_-^2}\right) \tag{A.1}$$

under the conditions

$$\sin^2 i_+ = 1 - \frac{\Lambda^2}{1-e_+^2} \geq 0\,, \tag{A.2}$$

$$\sin^2 i_- = 1 - \frac{\Lambda^2}{1-e_+^2} \leq 1\,. \tag{A.3}$$

Since $l \geq l_z$, we have $l_+ = \sqrt{1-e_-^2}$ and $l_- = max(\sqrt{1-e_+^2}, l_z)$. Assuming that the region of solutions is simply connected, we use the bisection method in order to obtain the value of e_+ and e_-.
However, there is an additional factor to consider. Librating orbits exist only if there exists a fixed point in the equation of motion for ω. Since librating orbits have their maximum/minimum angular momentum at $\omega = \frac{\pi}{2}$, this must be the value of ω at the fixed point. From equation 3.2,

$$\frac{3}{4l}\left(2l^2 + 5\left(\frac{l_z^2}{l^2} - l^2\right)\right) - \kappa l + \frac{B}{l^2} = 0 \tag{A.4}$$

must have a solution for l in $(0,1)$. This solution is called the fixed point angular momentum l_{fp}.

The loss cone in the traditional case is defined as $L_{lc} = \sqrt{2GM_1 r_t}$ where r_t is the tidal radius, and $l_{lc} = L_{lc}/L_c$. In the standard axisymmetric case, it is sufficient for $l_z < l_{lc}$ provided l can oscillate down to l_z. However, the presence of the secondary black hole breaks the z-axis symmetry, leading to oscillations of l_z on the timescale of the binary orbital period [3, 13]. The magnitude of these oscillations is given by

$$\Delta l_z = \frac{15}{8}\sqrt{\frac{3}{5}}q\left(\frac{a}{D}\right)^{3/2}\,. \tag{A.5}$$

Therefore, the effective size of the loss wedge is $l_t = l_{lc} + \Delta l_z$.
Thus. we have three conditions for a star to enter the loss wedge:

- l_+ and l_- must exist, and $l_+ > l_-$
- $0 \leq l_{fp} \leq 1$

- $l_- \leq l_t$

In figures A.1-A.3, we plot the values of $l_+, l_-, l_+ - l_-, l_{fp}$, and l_t for a fixed value of D, with $a \in (0, D/2]$.The other parameters are $M_1 = 10^7 M_\odot$, $q = 0.01$, $\eta r_0 = 1$pc, and $\gamma = 1.5$.

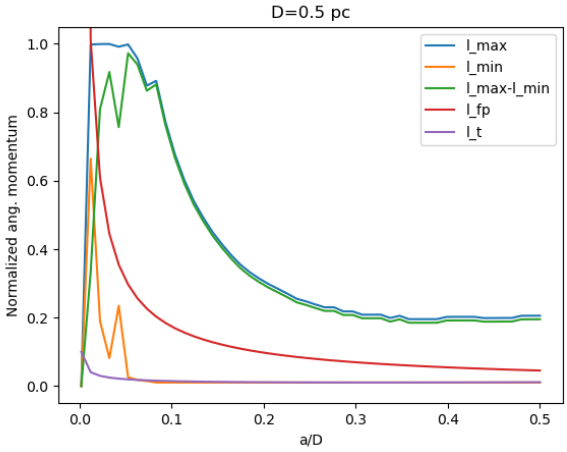

Figure A.1: $D = 0.5$ pc. We see that the conditions for the enhanced rate are satisfied for a partial range of a.

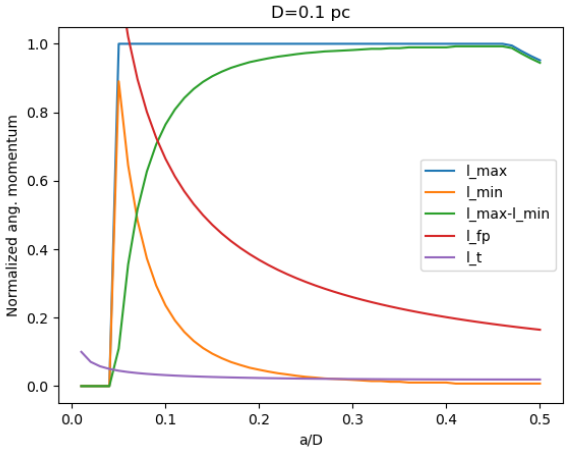

Figure A.2: $D = 0.1$ pc. We see that the conditions for the enhanced rate are satisfied for almost the full range of a.

In figures A.4 and A.5, we plot the same values for a range of D, with a being a fixed fraction of D. The other parameters are same as before.

Equation 3.39 reads

$$\frac{\dot{N}(t)}{\dot{N}_p} = 2^{5/2-p}\,(5/2-p)\left(\frac{D}{D_p}\right)^{-1/2-p}\int_0^{1/2}(l_+ - l_-)x^{3/2-p}dx\,. \tag{A.6}$$

Calling the value of the integral as $f(d)$, $d = D/D_p$, we plot the value of $f(d)$ as a function of d for various values of input parameters M_1, q, γ (or p), and r_h. We find that the function $f(d) = \frac{cd^b}{a+d^3} + k$ offers a good fit for $b \approx 1.5$, $a \approx 5.36$. c and k are of the order of $c \sim 10^{-1}$ and $k \sim 10^{-2}$ and are functions of the input parameters. The general trend of the value of c is increasing with increasing γ ($c \propto \gamma$), weakly dependent on q and M_1, and decreasing with increasing r_h ($c \propto r_h^{-0.5}$). Therefore we have

$$\int_0^{1/2}(l_+ - l_-)x^{3/2-p}dx \approx f(d, \gamma, q, M_1, r_h) = f(d)\,. \tag{A.7}$$

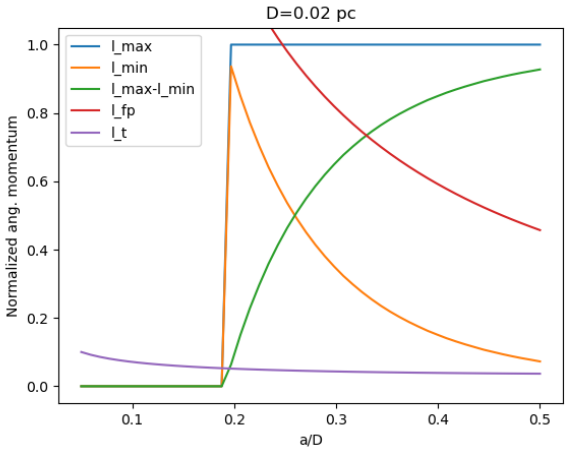

Figure A.3: $D = 0.02$ pc. We see that the conditions for the enhanced rate are not satisfied as $l_- > l_t$ for the entire range of a.

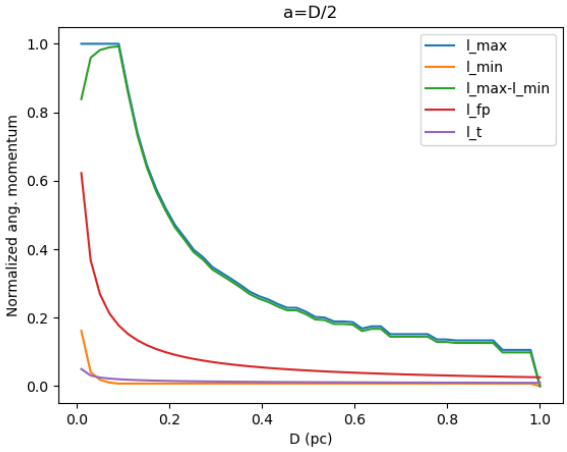

Figure A.4: $a = D/2$

Figure A.6 shows the value of $f(d)$ and the best fit curve for $M_1 = 1e7$, $q = 0.01$, $\gamma = 1.5$, and $r_h = 1$ pc.

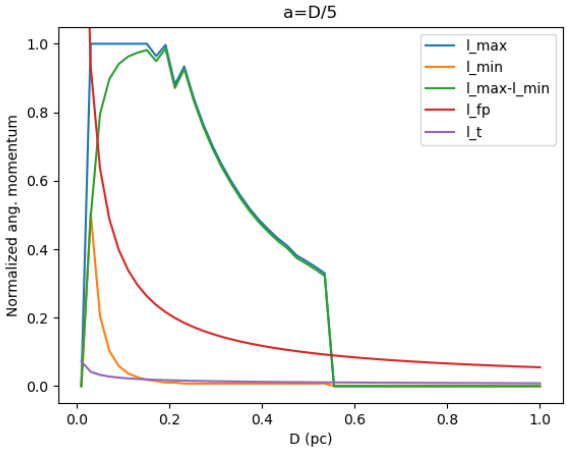

Figure A.5: $a = D/5$

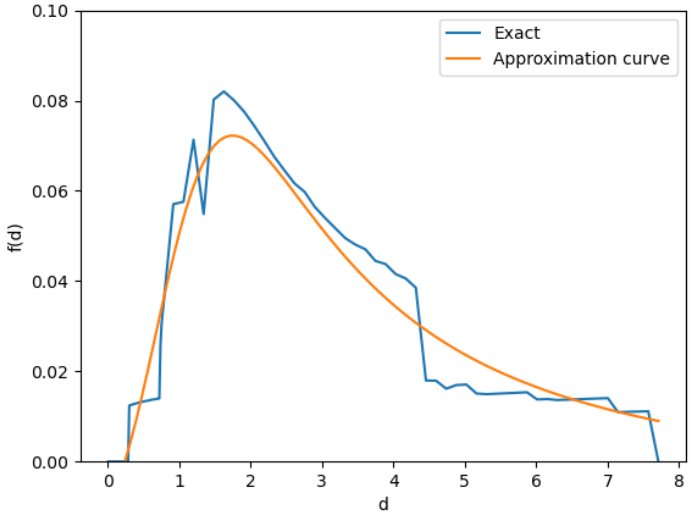

Figure A.6: $f(d)$ and best fit curve for $M_1 = 10^7 M_\odot$, $q = 0.01$, $\gamma = 1.5$, and $r_h = 1$ pc